Geophysical Journal International

Geophys. J. Int. (2011) doi: 10.1111/j.1365-246X.2011.05213.x

Insights into the 1968–1997 Dasht-e-Bayaz and Zirkuh earthquake sequences, eastern Iran, from calibrated relocations, InSAR and high-resolution satellite imagery

R. T. Walker,[1] E. A. Bergman,[2] W. Szeliga[3] and E. J. Fielding[3]

[1]*Department of Earth Sciences, University of Oxford, South Parks Road, Oxford,* OX1 3AN, *UK. E-mail: Richard.Walker@earth.ox.ac.uk*
[2]*Center for Imaging the Earth's Interior, Department of Physics, University of Colorado at Boulder,* 390 *UCB, CO* 80309, *USA*
[3]*Jet Propulsion Laboratory, California Institute of Technology,* 4800 *Oak Grove Drive, Pasadena, CA* 91109, *USA*

Accepted 2011 September 1. Received 2011 August 13; in original form 2011 March 10

SUMMARY

The sequence of seismicity in the Dasht-e-Bayaz and Zirkuh region of northeastern Iran, which includes 11 destructive earthquakes within a period of only 30 years, forms one of the most outstanding examples of clustered large and intermediate-magnitude seismic activity in the world. We perform a multiple-event relocation analysis, with procedures to remove systematic location bias, of 169 earthquakes, most of which occurred in the period 1968–2008, to better image the distribution of seismicity within this highly active part of Iran. The geographic locations of the clustered earthquakes were calibrated by the inclusion of phase arrivals from seismic stations at short epicentral distances, and also by matching the relative locations of the three largest events in the study to their mapped surface ruptures. The two independent calibration methods provide similar results that increase our confidence in the accuracy of the distribution of relocated epicentres. These calibrated epicentres, combined with the mapping of faults from high-resolution satellite imagery, and from an InSAR-derived constraint on fault location in one case, allow us to associate individual events with specific faults, and even with specific segments of faults, to better understand the nature of the active tectonics in this region during the past four decades. Several previous assumptions about the seismicity in this region are confirmed: (1) that the 1968 August 30 M_w 7.1 Dasht-e-Bayaz earthquake nucleated at a prominent segment boundary and left-step in the fault trace, (2) that the 1968 September 11 M_w 5.6 aftershock occurred on the Dasht-e-Bayaz fault at the eastern end of the 1968 rupture and (3) that the 1976 November 7 M_w 6.0 Qayen earthquake probably occurred on the E–W left-lateral Avash Fault. We show, in addition, that several significant events, including the 1968 September 1 and 4 (M_w 6.3 and 5.5) Ferdows earthquakes, the 1979 January 16 (M_w 6.5) and 1997 June 25 (M_w 5.9) Boznabad events and the 1979 December 7 (M_w 5.9) Kalat-e-Shur earthquake are likely to have ruptured previously unknown faults. Our improved description of the faulting involved in the 1968–1997 earthquake sequence highlights the importance of rupturing of conjugate left- and right-lateral faults in closely spaced events, or potentially even within a single earthquake, as was likely the case at the eastern end of the 1979 November 27 (M_w 7.1) Khuli-Buniabad main shock. The high level of clustered seismic activity probably results from the simultaneous activity on left- and right-lateral faults, an inherently unstable arrangement that must evolve rapidly. The combination of high-resolution satellite imagery and calibrated earthquake locations is a useful tool for investigating active tectonics, even in the absence of detailed field observations.

Key words: Interferometry; Seismicity and tectonics; Continental neotectonics; Continental tectonics: strike-slip and transform.

1 INTRODUCTION

On 1968 August 31, the western 80 km of the left-lateral Dasht-e-Bayaz Fault in northeastern Iran ruptured in an earthquake of M_w 7.1, killing an estimated 7000–12 000 people (e.g. Ambraseys & Tchalenko 1969; Tchalenko & Berberian 1975; Berberian & Yeats 1999; Walker *et al.* 2004). In the following 30 years, the region was subject to numerous further destructive earthquakes,

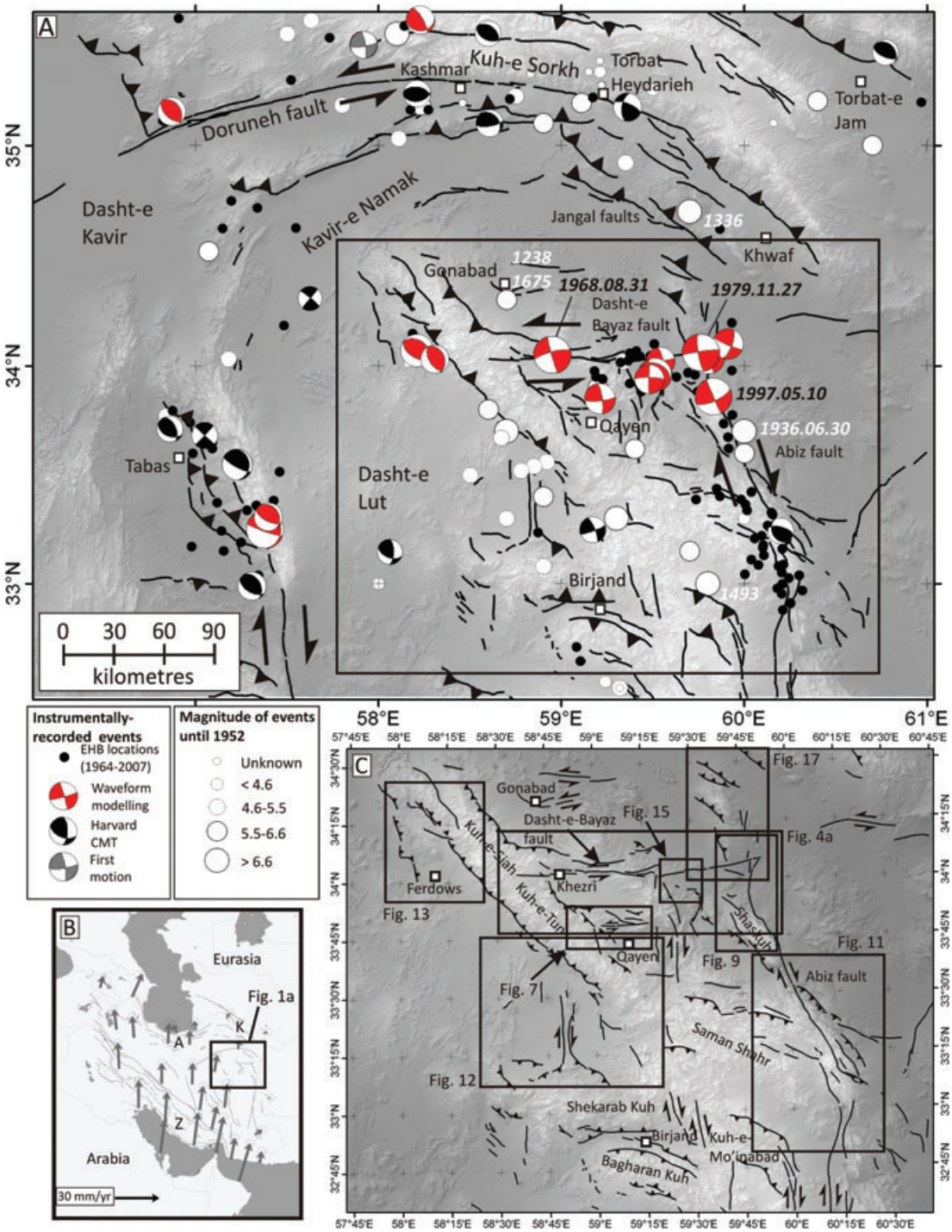

Figure 1. (a) Shaded-relief topographic map of the Dasht-e-Bayaz region (SRTM topography; Farr & Kobrick 2000). Fault-plane solutions of major earthquakes are from waveform modelling (red; listed in Jackson 2001), the Harvard CMT catalogue (black; http://www.globalcmt.org/) and from first motions (grey; McKenzie 1972). The epicentres of historical earthquakes occurring before 1952 are shown as white circles scaled by their inferred magnitude (Ambraseys & Melville 1982). (b) Map of Iran with GPS velocities of points relative to Eurasia from Vernant *et al.* (2004). Z = Zagros; A = Alborz; K = Kopeh Dagh. Both maps are in a Mercator projection. (c) Digital topographic map of the study region showing the active faults, main geographic features and with boxes showing the areas represented in later figures, see part (a) for location. This figure, and all later maps, are in a UTM zone 40 projection.

including four events of M_w 5.5–5.9, four events of M_w 6–6.9 and a further two large events of M_w 7+ (Fig. 1; Table 1). The first of the two later M_w 7 earthquakes, the Khuli-Buniabad earthquake of 1979 November 27 (M_w 7.1), ruptured the eastern 60 km of the Dasht-e-Bayaz Fault (Haghipour & Amidi 1980; Nowroozi & Mohajer-Ashjai 1980). The second, the 1997 May 10 M_w 7.2 Zirkuh earthquake, produced 125 km of surface ruptures on the N–S right-lateral Abiz Fault (Ikeda *et al.* 1998; Berberian *et al.* 1999; Sudhaus & Jónsson 2011). Together, the sequence of 11 destructive earthquakes forms one of the most outstanding examples of clustered large and

Table 1. Source parameters of instrumentally recorded earthquakes in the Dasht-e-Bayaz region that have been modelled using body waves (Walker *et al.* 2004). The epicentres are taken from the multiple-event locations listed in Table 2. References are: (1) Baker (1993), (2) Berberian *et al.* (1999), (3) Walker *et al.* (2003), (4) Jackson (2001) and (5) Walker *et al.* (2004). An 'm' in the M_w column signifies a multiple event. Centroid depth, strike, dip and rake of the modelled second subevent are listed for each multiple event (in italics). The subevent of the 1968 August 31 Dasht-e-Bayaz main shock that was placed ∼24 km east of the initial nucleation involved a mainly thrust mechanism on a fault striking NW–SE. The subevents, including that of the 1968 Dasht-e-Bayaz earthquake, are not included in the multiple-event locations and their focal mechanisms are not shown in the figures.

Date	Time	Lat.	Long.	Depth	M_w	Strike	Dip	Rake	Ref
1968.08.31	10:47	34.068	59.018	17	7.1m	254	84	5	5
				10	*6.4*	*320*	*70*	*90*	*5*
1968.09.01	07:27	34.099	58.155	9	6.3	115	54	85	3
1968.09.04	23:24	34.042	58.244	9	5.5	148	56	81	3
1968.09.11	19:17	34.031	59.472	6	5.6	78	90	16	1
1976.11.07	04:00	33.836	59.171	8	6.0m	84	79	12	1,4
				10		*67*	*52*	*−7*	*1*
1979.01.16	09:50	33.961	59.501	11	6.5m	293	34	46	1,4
				13		*257*	*88*	*5*	*1*
1979.11.14	02:21	34.017	59.780	10	6.6m	160	89	−177	1,4
				6		*85*	*85*	*1*	*1*
1979.11.27	17:10	34.056	59.769	8	7.1m	261	82	8	5
1979.12.07	09:24	34.130	59.889	10	5.9	113	84	21	1
1997.05.10	07:57	33.880	59.815	13	7.2	156	89	−160	2
1997.06.25	19:38	33.972	59.459	8	5.7	181	87	170	2

intermediate-magnitude seismic activity in the world (e.g. Berberian *et al.* 1999; Berberian & Yeats 1999). There is also an abundance of earthquakes around Dasht-e-Bayaz in the historical record (e.g. Ambraseys & Melville 1982; Berberian & Yeats 1999; Berberian & Yeats 2001, Fig. 1a), suggesting that the 20th century activity is part of a much longer sequence of destructive earthquakes in this part of Iran.

Despite the remarkable nature of the Dasht-e-Bayaz and Zirkuh earthquake sequence, and its potential importance in understanding the mechanisms of clustered earthquake activity, surprisingly little is known about the sources of several of the recent destructive events. In addition, understanding of the tectonic relationships of the earthquakes in this region has been hindered by difficulty in determining which of the many mapped faults have been active in specific earthquake sequences, because of poor control on epicentral locations using primarily teleseismic data. In this paper, we provide improved epicentral locations for 169 earthquakes within the region that help to constrain the details of these events. In conjunction with a detailed survey of active faulting from high-resolution satellite imagery, and with the source parameters of the larger earthquakes determined through body-waveform modelling (in other studies), we identify the probable faults responsible for the destructive earthquakes in the sequence, and also for many of the smaller events which occurred either as aftershocks or as background seismicity. In addition to improving our understanding of the fault sources responsible for the 1968–1997 earthquake sequence, our study also provides a framework that is useful in addressing the role of stress transfer in explaining why such a large number of clustered destructive earthquakes have occurred in this one small part of the world. These further investigations will be included in a separate, later paper.

2 TECTONIC SETTING

The active tectonics of Iran are controlled by the northward motion of Arabia, at a rate of ∼25 mm yr^{-1} at a longitude of 56°E, relative to Eurasia (Fig. 1b; Vernant *et al.* 2004). The GPS velocities of points relative to Eurasia decrease to zero at both the northern and eastern borders of Iran indicating that the major part of the continental shortening is confined within the political borders of Iran, with the majority of the deformation concentrated in the Zagros Mountains of southern Iran (Z in Fig. 1a), and in the Alborz and Kopeh Dagh mountains in the north (A and K in Fig. 1a).

The northward motion of central Iran relative to western Afghanistan results in regional-scale right-lateral shear across the eastern border of Iran. South of latitude 34°N this shear is accommodated on N–S right-lateral faults that surround the Dasht-e-Lut (e.g. Walker & Jackson 2004; Meyer & Le Dortz 2007; see Fig. 1a). North of latitude 34°N, however, the shear is accommodated by left-lateral shear on E–W trending faults that are thought to rotate clockwise about a vertical axis (see inset in Fig. 1b; Jackson & McKenzie 1984). The most prominent of the left-lateral faults are the Doruneh and Dasht-e-Bayaz faults (Fig. 1a).

The sequence of earthquakes that we investigated occurred in a region of transition between dominantly N–S right-lateral faulting (in the south) and E–W left-lateral faulting in the north (Fig. 1). The transition, which is likely to result from the orientations of inherited geological structures (e.g. Jackson & McKenzie 1984), results in relatively complicated arrangements and segmentation of active faults (e.g. Walker & Khatib 2006).

3 THE DASHT-E-BAYAZ EARTHQUAKE SEQUENCE

3.1 Overview

There is a long record of destructive earthquakes in northeast Iran (e.g. Ambraseys & Tchalenko 1969; Ambraseys & Melville 1982; Berberian & Yeats 1999; Berberian *et al.* 1999; Berberian & Yeats 2001; Walker *et al.* 2004). None of the pre-20th century events are assigned with certainty to individual faults, though the localized damage around Gonabad in the 1238 AD and 1675 AD events

strongly suggest the E–W Gonabad Fault as its origin (Fig. 1a). Likewise, an earthquake in 1493 AD generated a rupture that was documented at the time along a thrust at the margin of Kuh-e-Mo'inabad (Ambraseys & Melville 1982; Fig. 1a). Surface ruptures are attributed to events in 1936, 1941, 1947 and 1962 (Ambraseys & Melville 1982; Berberian *et al.* 1999).

The late 20th century sequence of earthquakes that is the subject of this study began with the 1968 August 30 Dasht-e-Bayaz earthquake (M_w 7.1), which involved predominantly left-lateral slip on the E–W Dasht-e-Bayaz Fault (e.g. Ambraseys & Tchalenko 1969; Tchalenko & Ambraseys 1970; Tchalenko & Berberian 1975). The eastern part of the Dasht-e-Bayaz fault ruptured in the (M_w 7.1) 1979 November 27 Khuli-Buniabad earthquake (e.g. Haghipour & Amidi 1980). None of the known historical events are thought to have ruptured the Dasht-e-Bayaz Fault.

The eastern part of our study area is defined by the right-lateral Abiz Fault, which trends south from its juncture with the Dasht-e-Bayaz Fault near 34°N, 59.8°E. The earliest known event on the Abiz Fault is the 1936 June 30 Abiz earthquake (M_s 6.0; Fig. 1a), which caused surface rupturing for a distance of 8–12 km along the central part of the Abiz Fault (Berberian *et al.* 1999). Two earthquakes in 1979 (the 1979 November 14 Korizan and 1979 December 7 Kalat-e-Shur events) are together thought to have ruptured ∼35 km of the northern Abiz Fault (e.g. Berberian *et al.* 1999), though, as we describe later, our results suggest that the Kalat-e-Shur earthquake actually occurred on an unmapped structure to the north of the Abiz Fault. The entire ∼125 km length of the Abiz Fault—including those parts that had recently broken in the 1936 and 1979 events—ruptured in the M_w 7.1, 1997 May 10 Zirkuh (also called the Ardekul) earthquake. No pre-20th century earthquakes are known to have ruptured the Abiz Fault, though Berberian *et al.* (1999) highlight several place names along it that might refer to pre-historic earthquake events.

In summary, four of the earthquakes in the 1968–1997 sequence (1968 August 30, 1979 November 14 and 27 and 1997 May 10) have been assigned to individual faults on the basis of definitive mapped surface rupture. Other fault-earthquake associations are less certain. An earthquake on 1947 September 23 is associated with ruptures on the Dustabad Fault that were visited ∼30 years after the event. Likewise, a series of right-lateral ruptures along the northern ∼10 km of the Abiz Fault are attributed either to a subevent of the predominantly left-lateral Khuli-Buniabad earthquake of 1979 November 27, or to the much smaller Kalat-e-Shur earthquake of 1979 December 7 (e.g. Haghipour & Amidi 1980; Ambraseys & Melville 1982; Berberian & Yeats 1999; Berberian *et al.* 1999). There are a number of intermediate magnitude events (e.g. 1968 September 1, 1968 September 4, 1968 September 11, 1976 November 7, 1979 January 16 and 1997 June 25) and a large number of smaller events for which the causative fault is unknown. The goal of this study is to use a combination of high-resolution satellite imagery and calibrated earthquake location to resolve some of these questions, and to better correlate the patterns of seismic rupture in this large and complex fault zone with geological expressions of large-scale deformation.

3.2 Calibrated relocation of epicentres

The assignment of earthquakes to specific faults or fault segments is a common goal for earth scientists, but inadequate location accuracy, especially for teleseismically observed earthquakes, can make the task challenging. Departure of the true velocity structure from the standard 1-D global velocity models used for earthquake location introduces both scatter and bias in earthquake epicentres unless there are seismic stations at very short range (e.g. Bondár *et al.* 2004), and location accuracy is even more compromised by the use of far-regional stations (as is common in Iran) than by teleseismic stations. Systematic location errors of up to 10–15 km have been reported in Iran (e.g. Berberian 1979; Ambraseys 2001) and comparisons with calibrated earthquake locations in Iran indicate that the 90 per cent accuracy level is 20 km or more for all standard catalogues (manuscript in preparation). Given that the active faults in Iran are often separated by only 10–15 km, the uncertainty in epicentral location often precludes a confident identification of the causative fault using standard catalogue locations. In recent years, however, techniques have been developed to minimize the scatter and bias in earthquake locations from unknown Earth's structure, often achieving a location accuracy of less than 5 km. We use one such technique here to obtain epicentral locations that can be more confidently associated with faults that have been identified by field mapping and high-resolution satellite imagery.

Our relocation method is based on the hypocentroidal decomposition (HDC) method for multiple-event relocation (Jordan & Sverdrup 1981), with extensive development and testing for use in determining earthquake locations for which scatter and bias have both been minimized. We refer to such locations as 'calibrated', a term that properly refers only to the minimization of location bias. The method has been applied in a number of studies (Ritzwoller *et al.* 2003; Bondár *et al.* 2004; Walker *et al.* 2005; Biggs *et al.* 2006; Parsons *et al.* 2006; Tatar *et al.* 2007; Bondár *et al.* 2008; Nissen *et al.* 2010).

Like all multiple-event relocation methods, HDC makes use of the fact that the ray paths of a given phase for two or more members of a cluster of earthquakes, observed at a distant station, will largely sample the same portion of the Earth. Therefore, the error from unmodelled Earth's structure along the paths is highly correlated and the difference in those traveltimes mostly reflects the events' relative location. The distinguishing feature of the HDC algorithm, and the one that makes it particularly suitable for research on calibrated locations, is the HDC theorem (Jordan & Sverdrup 1981) which describes how the location problem for a cluster of seismic sources can be decomposed into two separate problems, the estimation of the following:

(1) The 'hypocentroid', which is a virtual event with hypocentral coordinates given by the average of the corresponding coordinates of all the events in the cluster. The hypocentroid is described in absolute coordinates: geographic latitude and longitude, depth below mean sea level and UT for origin time.

(2) The 'cluster vectors', which describe the location of each event with respect to the current hypocentroid. Cluster vectors are defined in local coordinates; kilometres north and south, kilometres above or below, and seconds before or after the hypocentroid.

The HDC theorem also points to a method of solution, based on the fact that improved cluster vectors can be estimated separately from the hypocentroid, using traveltime differences. Then, a new hypocentroid can be estimated, using absolute traveltimes from all events in the cluster as if it were associated with the hypocentroid 'event'. Absolute locations of all cluster events are updated by adding the cluster vectors to the new hypocentroid. This two-step process is repeated to convergence, usually in two or three iterations. Projection operators handle the difficult task of decomposing the arrival time data set into the matrices needed for inversion, and they have the desirable qualities that all information in the data set that bears on the relative locations of any events in the cluster is

guaranteed to be carried through, along with the information on data uncertainty that ultimately controls the estimate of location uncertainty.

The great advantage of the HDC algorithm for research in calibrated locations lies in the fact that it is not required that the same data be used for estimation of the cluster vectors and the hypocentroid. For cluster vectors, the dependence on traveltime differences precludes the use of any arrival time reading for which there is no other observation of that phase at that station. Beyond that requirement, more data are better, as long as it is properly weighted. Data from stations at all epicentral distance can be used and secondary phases can be used despite the fact that theoretical traveltimes are known to have baseline errors for many of them.

For the estimate of the hypocentroid, which ultimately controls the bias in all locations, we want to be very careful about the data used. A reasonable result (better than most single-event locations) can be achieved using teleseismic (30°–90° epicentral distance) *P* arrivals alone. This part of the standard traveltime model (ak135) is the most reliable, globally. However, locations determined this way are known to have uncertainties of 10 km or more, and are still subject to bias because of the uneven distribution of seismic stations with respect to most source regions (including the study area in northeastern Iran). Ultimately, the only way to remove bias from earthquake locations, in the absence of a perfect earth model, is to estimate the location using arrival time data that are not sampling large portions of the Earth. We have developed two ways to do this.

(1) 'Direct Calibration' estimates the hypocentroid using only arrival time data from stations at short epicentral distances. The amount of traveltime error (relative to our theoretical model) that can accumulate over a short path is limited. In most cases, we restrict the data used in this approach to direct-arriving *P* and *S* phases at distances less than the Pg-Pn crossover distance, which is typically about 200 km in the study region.

(2) 'Indirect Calibration' carries out the HDC analysis using teleseismic *P* arrivals to estimate the hypocentroid, but then corrects the location of the cluster by reference to one or more 'calibration events' that provide independent information on some or all of the coordinates of one or more members of the cluster. Because the relative locations of all cluster events are constrained by the HDC analysis, the entire cluster is shifted in space and time to match the available calibration data. Calibration data can be derived from several types of sources: locations of a subset of cluster events determined from dense local networks, such as aftershock surveys, mapped faulting which is reliably associated with a known earthquake, information on surface displacement from shallow events through InSAR analysis (e.g. Lohman & Simons 2005a) and other types of remote sensing.

In this study, we employ both direct and indirect calibration, and they are in good agreement, but the listed locations will be based on indirect calibration because the uncertainties are somewhat smaller.

3.3 Selection of earthquakes

The 169 events used in our analysis were extracted from a database of earthquake locations in the Iran region, located with the EHB single-event location algorithm of Engdahl *et al*. (1998). In assembling this catalogue, most of the events have been carefully reviewed for proper phase identification, flagging of outliers (readings with unacceptably large residuals against a reference traveltime model) and analysis of depth phases. Unlike the well-known global EHB catalogue based on these procedures, the Iran catalogue has not been filtered to remove events with poor azimuthal coverage. We rely on the HDC analysis to reveal events whose locations cannot be constrained sufficiently for our purposes. In some cases, events with rather large open azimuth can be located to a useful level of accuracy in the multiple-event analysis. Also, during the HDC analysis, we will perform a considerably more detailed analysis of outlier readings, change some phase identifications and re-examine the depth phases.

The Iran catalogue contains instrumentally recorded events from 1923 to 2008. For the Dasht-e-Bayaz and Zirkuh study region, we have an event as old as 1947 but most events are between 1968 and 2008. The magnitude at which the catalogue is complete varies greatly through time, as a function of the increasing density of seismic stations around the world and even more so in Iran itself. Widespread deployment of permanent local and regional seismic networks in Iran began in the mid-1990s and accelerated after 2000. In recent years, we are often able to obtain reliable locations for events of around magnitude 3.5 and above. For the earlier part of our earthquake set, from the late 1960s to the 1990s, the completeness level is probably decreasing slowly from about magnitude 5 to perhaps 4.5. These variations must be kept in mind when reviewing the resulting seismicity patterns.

In our HDC analysis, focal depths are normally fixed. It is quite rare to obtain a data set of earthquake arrival times that includes adequate recording of depth phases and/or very close stations to constrain the depth of all events in the cluster. Without such connectivity, the system of equations is singular. About 40 per cent of the events in the cluster have reported depth phases that can be used to constrain focal depths, and this has been done in the single-event location procedure used in constructing the Iran catalogue from which these data are extracted. On this basis, plus reference to body-waveform studies when they are available, a range of depths from 5 to 15 km was estimated, which is consistent with a detailed study of focal depths across the Iran region (Engdahl *et al.* 2008). In the course of HDC analysis, we have further refined some of these depths. We have used a default depth of 12 km for the HDC analysis. Differences in assumed depth of less than about 10 km have a very small effect on the epicentre unless there are stations at extremely short range.

3.4 Direct calibration

For direct calibration, we depend on short path lengths to minimize error in our theoretical traveltimes, but we wish to have as accurate a local model as possible. Theoretical traveltimes for crustal (Pg, Sg) phases are calculated with a simple plane-layered model whose *P* and *S* velocities are adjusted to fit the distance dependence of arrival time data in the source region. For a single event with a dozen or so readings this approach would not be possible, because the event's location would trade-off with the velocity model, but with hundreds of readings from multiple events whose relative locations are fixed it is a fairly stable procedure. The fit to Pg and Sg arrivals at very short range (if they are available) also provides information on the depths of the cluster events contributing the data. The thickness of the crust and the velocity of the upper-mantle half-space are then adjusted to fit the Pn and Sn arrivals. The data available for direct calibration of the Dasht-e-Bayaz/Zirkuh cluster have epicentral distances ranging from about 10 to 190 km. The arrival times of Pg and Sg in this distance range can be fit very well with a single-layer crust with velocities of 6.1 and 3.4 km s^{-1} (Fig. 2). The Pn arrival times are

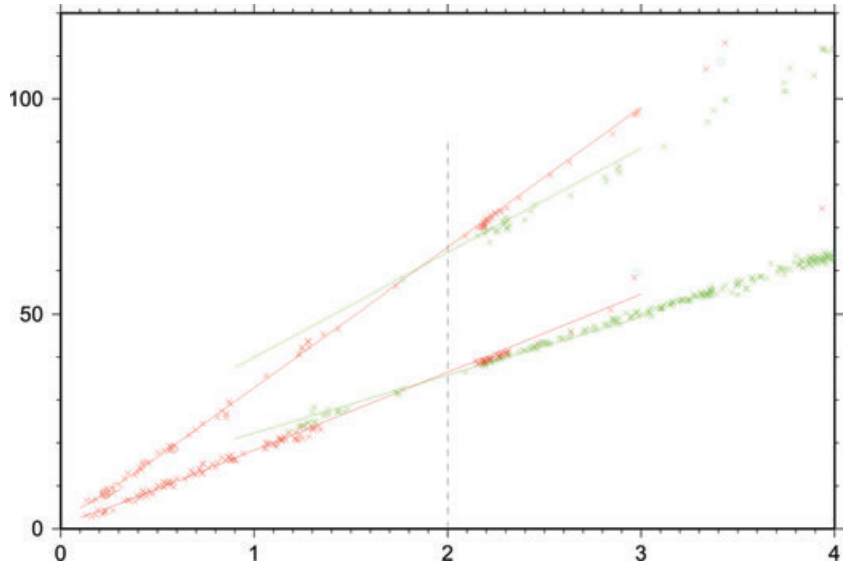

Figure 2. Fit of observed local (Pg and Sg) and near-regional (Pn and Sn) arrivals to traveltimes predicted for a single-layer crustal layer (6.1 and 3.4 km s^{-1}, 46 km thick) over a half-space (8.15 km s^{-1}, 4.55 km s^{-1}). The dashed line shows the cut-off distance for data used in direct calibration.

very well matched with a crustal thickness of 46 km and velocity of 8.15 km s^{-1}, but the optimal value of crustal thickness depends on the assumed depths of the earthquakes. An upper-mantle *S* velocity of 4.55 km s^{-1} provides a reasonable match to observed Sn arrivals at shorter distances.

The Pg-Pn crossover distance with this model and the assumed source depths is at about 1.8°, but there is not a significant difference between the two traveltime curves (such that a misidentification of the phase name could lead to location bias) until beyond 2.0°. Although we used 2.0° epicentral distance as the cut-off for use in estimating the hypocentroid, the furthest station within this range is at about 1.8°. As can be seen in Fig. 2, a small number of Pn arrivals, seen as secondary arrivals, are used in addition to Pg for estimating the hypocentroid. Such back-branch Pn arrivals are often seen in similar studies of Iranian earthquake clusters. Both Pg and Pn are sometimes reported in Iranian network bulletins and we have seen them ourselves when picking arrival times.

The direct calibration of the Dasht-e-Bayaz/Zirkuh cluster is accomplished with 174 readings, mostly Pg and Sg, which yields a location for the hypocentroid with a confidence ellipse equivalent to a circle of about 4.55 km radius (semi-axis lengths of 4.4 and 4.7 km). All confidence ellipses reported in this study are calculated at the 90 per cent level. The ray paths used for direct calibration are shown in Fig. 3. The readings come from four separate networks operated in the region: (1) The Iran Telemetered Seismic Network (ITSN) operated by the Institute of Geophysics, University of Tehran (data available through their website: http://irsc.ut.ac.ir/); (2) The Iran Strong Motion Network (ISMN), operated by the Building and Housing Research Centre (BHRC). Some information is available through their website (http://www.bhrc.ac.ir/ISMN/Index.htm), but data acquisition requires direct communication with BHRC staff. The BHRC instruments did not have calibrated timing systems and we could only use the *S-P* times for location, but they only trigger at close distances so they provide quite good constraint on location and depth; (3) The Khorasan Seismic Network (KHSN), operated by the Earthquake Research Center (EQRC), Ferdowsi University in Mashad. Although some information is available through their website (http://seismo.um.ac.ir/), data acquisition requires direct communication with EQRC staff; (4) A temporary deployment for

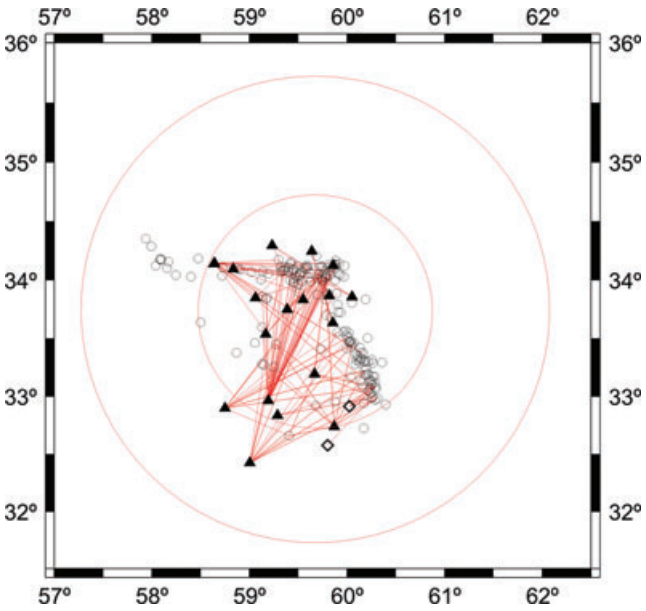

Figure 3. Ray paths used to locate the hypocentroid of the Dasht-e-Bayaz/Zirkuh cluster in direct calibration. Open circles are earthquakes in the cluster. Solid triangles represent seismic stations. Open diamonds are stations operating strong motion instruments without calibrated timing; *S-P* times from these stations are used to help constrain locations. Circles are at radii of 100 and 200 km.

aftershock studies after the Khuli-Buniabad earthquake in 1979 by the Atomic Energy Agency of Iran (AEI), the forerunner of the Atomic Energy Organization of Iran (AEOI). Data for three events in our cluster were published in an unpublished internal report.

Although the density and variety of orientations of the ray paths are impressive, the distribution of data in azimuth is rather unbalanced, with azimuths (event to station) in the west and southwest being overly weighted. When the uncertainty of relative location for each event is added to this hypocentroidal uncertainty, few of the events would have location uncertainties of 5 km or less. In hope

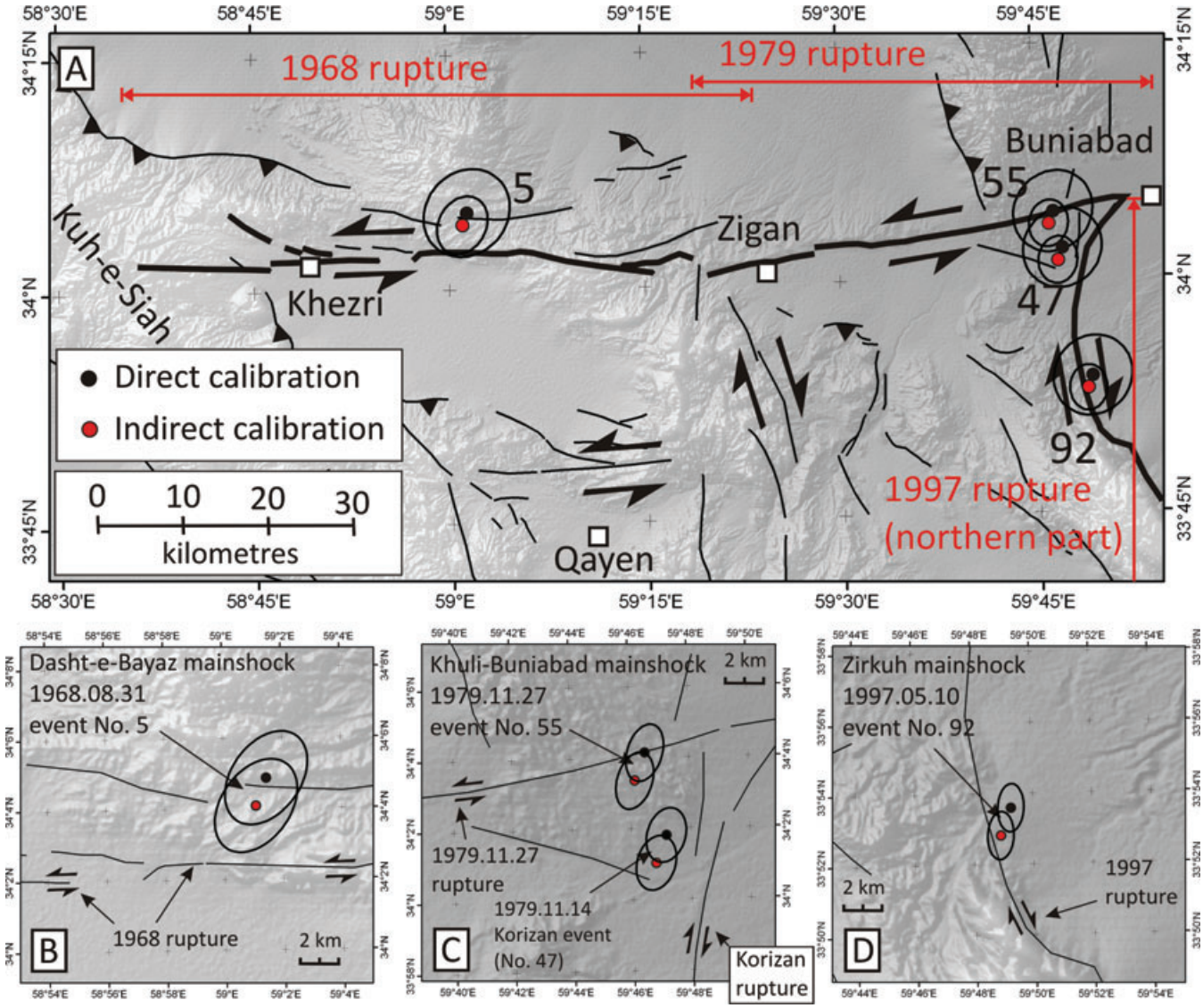

Figure 4. Locations of the three main shocks used for indirect calibration. The solid black circles represent epicentres determined by direct calibration (see Section 3.4). Solid red circles represent those from indirect calibration (Section 3.5). Relative locations are extracted from the relocation of the entire cluster of 169 events (Table 2). For the indirect calibration, the location of the 1997 May 10 Zirkuh main shock (#92, M_w 7.2) is set so that its epicentre is consistent with the longitude of the mapped surface faulting and the 1968 August 31 Dasht-e Bayaz and 1979 November 27 Khuli-Buniabad main shocks (#5 and 55, respectively, both M_w 7.1) are consistent with the latitude of their respective mapped surface faulting along the Dasht-e Bayaz fault. Event #47, the M_w 6.6 Korizan event on 1979 November 14, was not used for indirect calibration, but its epicentre is tightly constrained to be a few kilometres south of the epicentre of the Khuli-Buniabad event. The lower panels (b)–(d) show close-up views of all three of the calibration events. The 90 per cent confidence ellipses shown in these lower panels are for the cluster vector (i.e. relative location). These ellipses are smaller than the confidence ellipses shown in the upper panel and listed in Table 2, which include the uncertainty in both the hypocentroid location and the cluster vectors. The difference in location between directly and indirectly calibrated epicentres is only 1.5 km and is well within the uncertainty of either calibration method.

of obtaining a result with smaller confidence ellipses on location, we also performed a calibration of the cluster using the indirect method.

3.5 Indirect calibration

In the case of the Dasht-e-Bayaz sequence, the faults responsible for the three $M_w > 7$ main shocks provide a means of constraining the location of the cluster because they occur on steeply dipping strike-slip faults, which are orthogonal to each other. Coseismic ruptures are well documented on the E–W trending Dasht-e-Bayaz Fault for the 1968 Dasht-e-Bayaz and 1979 Khuli-Buniabad earthquakes, and on the N–S trending Abiz Fault for the 1997 Zirkuh event (Fig. 4).

Preliminary uncalibrated relocation of the earthquake cluster yields very tight constraints on the relative locations of the main shocks, because they share a large number of observations by the same stations. Calibration for latitude is done by requiring the 1968 and 1979 events to be consistent with the surface expression of co-seismic faulting, taking into consideration their focal mechanisms. The fault planes for both events dip slightly to the north (84° and 82°, respectively, Table 1), so the epicentres are expected to be slightly to the north of the surface traces of faulting. The relative locations of these two events, however, requires the epicentre of

the 1979 event to be relatively a few kilometres south of the 1968 event. Our calibration splits the difference, placing the 1968 event slightly further north than otherwise, that of the 1979 event slightly south (Figs 4b and c). In fact, the appropriate latitude for the 1979 event is somewhat in doubt. The field study that found the surface trace shown in Fig. 4(c) was not exhaustive and did not explore the possibility of additional fractures to the south. Given the evident complexity of faulting in this region, a teleseismic epicentre slightly south of the mapped trace does not overly disturb us.

Given the latitude inferred from the earlier analysis, the longitude of the calibrated cluster is set by requiring the epicentre of the 1997 Zirkuh event to lie on the mapped surface trace of coseismic faulting (Fig. 4d). This event's focal mechanism features a near-vertical (89°) fault plane and there is little ambiguity about the location of the surface trace of primary faulting, so no significant offset from the surface faulting is expected. We note that InSAR modelling suggests a westward dip of 75°–80° on the fault at the latitude of the epicentre (Sudhaus & Jónsson 2011) such that an epicentre 1–2 km west of the fault trace could be possible.

In order for the final epicentral accuracy for all cluster events to be properly estimated, the uncertainties of the calibration data must be carried through the relocation process and added to the uncertainties of the cluster vectors that describe the relative locations of all events in the cluster. The uncertainty of the estimation process for the hypocentroid in the HDC analysis is irrelevant in this case, because that estimate of the hypocentroid will be shifted to match the calibration data. For simplicity, we encapsulated the calibration information derived from the mapped faulting of the three main shocks discussed earlier into a single calibration location, for the 1997 Zirkuh event. This is represented by a covariance matrix that is equivalent to a 90 per cent confidence ellipse that is a circle of 2 km radius.

The results with indirect calibration are in close agreement with those from direct calibration (Fig. 4). After direct calibration, the additional shift required to bring the cluster into alignment with the calibration locations described above is 1.5 km at an azimuth of 201°, well within the uncertainty of the calibration using either method. We report the locations and uncertainties based on indirect calibration because the uncertainty of indirect calibration is better, 2.3 km versus 4.5 km if the confidence ellipses are converted to a circle of equivalent area.

The calibrated locations of all events, with confidence ellipses and the change in location from the original single-event locations, are shown in Fig. 5. Of 169 events, 118 have confidence ellipses smaller than 5 km. When inferring the association of an event with any geological feature, the full confidence ellipse must be taken into account. When comparing the relative locations of two or more events in the cluster, the confidence ellipses for the cluster vectors (which are always smaller than the full confidence ellipse) are the relevant measure of location uncertainty, and in a few figures where the emphasis is on relative locations or clustering we have shown the cluster vector confidence ellipses. The locations of all 169 events are listed in Table 2.

Except for the first four events, which are widely scattered in both time and place, all events in the relocated cluster are divided into seven sequential subclusters, listed in Table 3, which are each

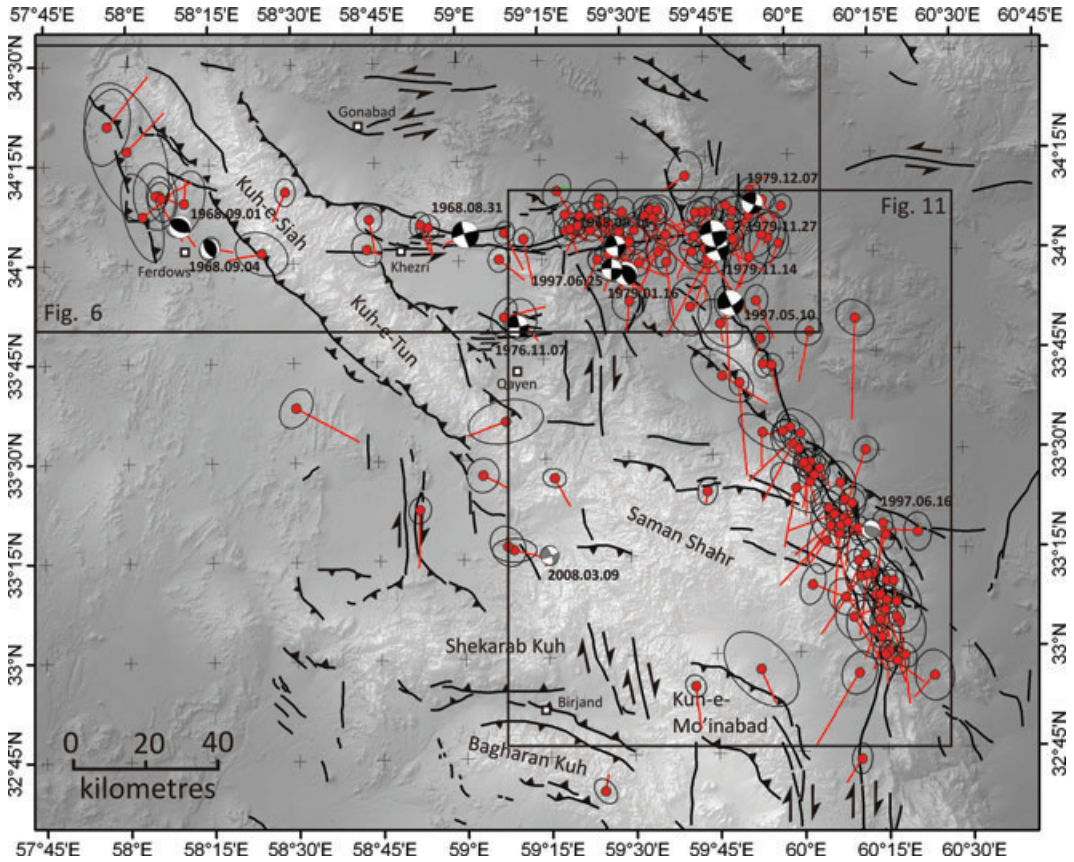

Figure 5. Epicentres of earthquakes in the Dasht-e-Bayaz and Zirkuh region. The red circles are epicentres determined from indirect calibration (see Section 3.5). Each location is shown with its 90 per cent confidence ellipse. The red bars link each epicentre with its initial single-event location. The effect of relocation is generally to tighten the clustering of epicentres.

Table 2. Calibrated epicentres of earthquakes in the study region determined with the methods described in Section 3. For most events of magnitude less than about 5.0, the International Seismological Centre (ISC) body-wave magnitude (m_b) is used, as it is based on the largest number of readings and is consistent throughout the period of interest. Moment-magnitude (M_w) has been determined for most of the events larger than 5.0 (from Baker 1993; Walker *et al.* 2003; Walker *et al.* 2004; HRVD, Harvard; NEIC, USGS National Earthquake Information Center). Surface wave magnitude (M_s) is used for several older events (PAS Seismological Center, Pasadena; KIR, Kiruna, Sweden; UPP, Uppsala Seismological Institute; MOS, Moscow Institute of Physics of the Earth). For some recent, and very small, events, only M_L magnitudes are available and we have listed the CSEM (Centre Sismologique Euro-Mediterraneen) estimates of those. A1 and A2 are the azimuths in degrees, clockwise from north, of the semi-axes of the 90 per cent confidence ellipse for the epicentre. L1 and L2 represent the lengths of the corresponding semi-axes in kilometres. Area is the area in km^2 of the 90 per cent confidence ellipse. Those events for which body-waveform solutions are available (Table 1) are shown in bold.

No.	Date	Time (GMT)	Lat.	Long.	Dep.	Mag.	Mag. type & source	A1	L1	A2	L2	Area
1	1947.09.23	12:28:13.27	33.636	58.499	12	6.8	M_s (PAS)	302	4.1	32	5.9	75
2	1962.04.01	00:45:09.91	33.375	58.867	12	5.8	M_s?(KIR, UPP, MOS)	285	3.1	15	3.8	36
3	1964.02.21	01:03:57.62	34.35	57.936	12	4.9	m_b (ISC)	283	6.2	13	10.9	212
4	1968.07.31	20:04:58.39	33.834	60.19	12	4.3	m_b (ISC)	40	4.6	130	5.7	84
5	**1968.08.31**	**10:47:37.20**	**34.068**	**59.018**	**10**	**7.1**	**M_w (Walker)**	**299**	**2.8**	**29**	**3.6**	**32**
6	1968.08.31	11:34:31.27	34.07	59.136	9	5.4	m_b (ISC)	294	2.8	24	3.3	29
7	1968.08.31	13:22:56.32	34.151	59.426	8	4.7	m_b (ISC)	314	4.4	44	5.9	81
8	1968.08.31	14:06:15.93	34.071	59.322	12	4.9	m_b (ISC)	276	3.2	6	4.1	42
9	**1968.09.01**	**07:27:29.68**	**34.099**	**58.155**	**12**	**6.3**	**M_w (Walker)**	**288**	**2.5**	**18**	**2.9**	**23**
10	1968.09.01	08:23:14.43	34.287	57.995	12	5.2	m_b (ISC)	71	10.2	161	20.4	654
11	1968.09.01	11:03:58.59	34.042	59.932	12	4.9	m_b (ISC)	286	4.8	16	7.4	112
12	1968.09.01	19:16:35.58	34.176	58.09	12	4.8	m_b (ISC)	287	2.9	17	3.9	36
13	1968.09.01	21:16:37.98	34.122	58.041	12	4.8	m_b (ISC)	74	5.0	164	12.8	199
14	1968.09.03	09:53:47.20	34.003	59.119	12	4.9	m_b (ISC)	281	3.0	11	3.5	33
15	1968.09.04	08:08:42.57	34.079	59.354	12	5.0	m_b (ISC)	81	3.4	171	4.2	46
16	1968.09.04	11:19:34.07	34.053	59.194	12	5.0	m_b (ISC)	271	2.8	1	3.2	28
17	**1968.09.04**	**23:24:46.70**	**34.042**	**58.244**	**12**	**5.5**	**M_w (Walker)**	**295**	**2.7**	**25**	**3.3**	**28**
18	1968.09.06	02:27:35.54	34.106	59.397	16	4.7	m_b (ISC)	276	4.0	6	4.2	53
19	1968.09.10	20:31:58.44	34.112	59.32	12	4.7	m_b (ISC)	273	3.2	3	3.8	38
20	**1968.09.11**	**19:17:10.41**	**34.031**	**59.472**	**12**	**5.6**	**M_w (Baker)**	**290**	**3.0**	**20**	**3.8**	**36**
21	1968.09.15	09:42:13.32	34.109	59.364	12	4.8	m_b (ISC)	86	3.6	176	3.8	43
22	1968.09.17	19:15:06.11	34.027	58.401	12	4.4	m_b (ISC)	28	5.7	118	7.7	138
23	1968.09.19	05:15:09.34	34.175	58.081	12	4.5	m_b (ISC)	85	6.1	175	9.4	179
24	1968.10.13	01:34:49.30	34.033	58.72	12			59	3.9	149	4.9	60
25	1968.11.28	18:02:44.03	34.203	59.687	12	4.8	m_b (ISC)	279	4.9	9	6.9	106
26	1969.08.23	19:16:15.47	34.087	58.905	12	4.9	m_b (ISC)	88	3.3	178	3.6	37
27	1969.09.03	23:38:59.53	34.155	58.168	12	4.9	m_b (ISC)	288	5.3	18	9.6	159
28	1969.12.02	22:46:12.83	34.109	58.727	12	5.0	m_b (ISC)	61	3.7	151	3.8	44
29	1970.03.01	20:12:41.80	34.093	58.882	12	5.0	m_b (ISC)	279	2.9	9	3.7	34
30	1970.03.17	23:19:41.52	34.117	59.493	11	4.9	m_b (ISC)	293	3.6	23	4.0	45
31	1974.02.16	06:07:46.63	34.168	58.098	12			82	3.9	172	6.4	79
32	**1976.11.07**	**04:00:51.07**	**33.836**	**59.171**	**12**	**6.0**	**M_w (Baker)**	**281**	**2.4**	**11**	**2.9**	**22**
33	1976.11.09	17:59:51.76	33.857	59.131	12	5.1	m_b (ISC)	289	3.4	19	5.6	60
34	1977.03.19	03:29:06.89	33.851	59.18	12	4.7	m_b (MOS)	273	4.6	3	5.8	83
35	1977.11.10	13:52:33.90	34.077	59.335	12	4.6	m_b (ISC)	280	2.8	10	3.1	27
36	**1979.01.16**	**09:50:07.06**	**33.961**	**59.501**	**13**	**6.5**	**M_w (Baker)**	**280**	**2.3**	**10**	**2.8**	**21**
37	1979.01.16	13:45:26.66	34.097	59.592	12	4.6	m_b (ISC)	274	3.3	4	5.6	59
38	1979.01.17	07:52:40.49	34.07	59.529	12	4.7	m_b (ISC)	87	3.0	177	4.8	45
39	1979.01.18	00:24:59.58	33.987	59.541	12	5.0	m_b (ISC)	270	2.8	0	3.7	33
40	1979.01.19	19:29:42.29	33.998	59.416	12	5.1	m_b (ISC)	271	2.6	1	3.2	26
41	1979.01.21	18:59:49.41	33.982	59.448	12	4.3	m_b (ISC)	28	3.9	118	5.9	72
42	1979.01.27	05:32:44.78	34.014	59.6	12	4.4	m_b (ISC)	85	3.3	175	4.6	48
43	1979.02.03	21:47:21.49	34.047	59.514	12	4.1	m_b (ISC)	357	4.5	87	5.6	80
44	1979.02.08	13:36:08.25	34.019	59.49	12	4.4	m_b (ISC)	281	3.6	11	5.2	58
45	1979.04.23	17:24:16.25	33.892	59.51	12	4.6	m_b (ISC)	288	4.7	18	5.5	81
46	1979.08.25	13:46:24.13	33.594	59.13	12	4.1	m_b (ISC)	349	6.0	79	10.6	199
47	**1979.11.14**	**02:21:18.93**	**34.017**	**59.78**	**12**	**6.6**	**M_w (Baker)**	**279**	**2.3**	**9**	**2.8**	**20**
48	1979.11.14	02:50:14.93	34.05	59.914	12	4.8	m_b (ISC)	304	4.3	34	7.0	96
49	1979.11.14	04:18:23.37	34.038	59.792	12	4.7	m_b (ISC)	350	4.2	80	5.1	67
50	1979.11.14	07:43:36.31	34.018	59.742	12	4.5	m_b (ISC)	336	3.6	66	4.1	47
51	1979.11.15	03:25:26.46	33.998	59.749	14	4.8	m_b (ISC)	75	2.8	165	3.1	28
52	1979.11.15	05:06:52.19	34.041	59.827	12	4.9	m_b (ISC)	81	3.2	171	3.4	34
53	1979.11.23	18:22:45.89	34.125	59.87	12	5.0	m_b (ISC)	283	2.4	13	2.9	22
54	1979.11.27	07:12:35.54	34.099	59.878	12	5.1	m_b (ISC)	284	2.5	14	3.3	26
55	**1979.11.27**	**17:10:32.62**	**34.056**	**59.769**	**10**	**7.1**	**M_w (Walker)**	**281**	**2.3**	**11**	**2.8**	**20**

Table 2. (*Continued.*)

No.	Date	Time (GMT)	Lat.	Long.	Dep.	Mag.	Mag. type & source	A1	L1	A2	L2	Area
56	1979.11.27	18:04:58.58	34.102	59.585	12	4.6	m_b (ISC)	314	3.5	44	4.4	49
57	1979.11.27	20:00:16.15	34.039	59.514	12	4.3	m_b (ISC)	322	6.2	52	8.7	171
58	1979.11.27	20:48:25.54	33.995	59.876	12	4.2	m_b (ISC)	300	4.8	30	8.0	121
59	1979.11.27	23:14:57.45	34.084	59.455	12	4.5	m_b (ISC)	81	3.1	171	3.6	36
60	1979.11.28	03:56:49.62	34.131	59.873	12	4.7	m_b (ISC)	314	2.8	44	3.4	30
61	1979.11.28	11:55:52.04	34.112	59.752	12	4.1	m_b (ISC)	327	4.0	57	4.5	57
62	1979.11.28	16:38:40.52	34.091	59.439	12	3.9	m_b (ISC)	0	4.1	90	5.9	76
63	1979.11.28	18:09:14.16	34.112	59.827	12	4.3	m_b (ISC)	339	3.7	69	5.8	67
64	1979.11.28	19:09:48.59	34.112	59.735	12	4.4	m_b (ISC)	317	3.7	47	4.6	54
65	1979.11.29	00:48:55.27	34.067	59.482	12	4.4	m_b (ISC)	300	3.6	30	3.8	43
66	1979.11.30	20:49:04.18	34.028	59.965	12	4.5	m_b (ISC)	285	2.8	15	4.3	37
67	1979.12.02	21:09:34.59	34.051	59.709	12	4.1	m_b (ISC)	44	2.8	134	3.2	27
68	**1979.12.07**	**09:23:57.41**	**34.13**	**59.889**	**12**	**5.9**	**M_w (Baker)**	**278**	**2.3**	**8**	**2.6**	**19**
69	1979.12.07	09:54:47.55	34.138	59.919	12	4.8	m_b (ISC)	9	2.9	99	3.7	34
70	1979.12.07	10:45:04.93	34.164	59.882	12	4.8	m_b (ISC)	85	2.9	175	3.2	30
71	1979.12.11	02:16:58.83	34.011	59.702	12	4.4	m_b (ISC)	53	3.0	143	3.8	36
72	1979.12.16	22:35:37.33	34.084	59.359	12	5.0	m_b (ISC)	86	2.4	176	2.7	21
73	1979.12.20	10:24:23.84	34.011	59.449	12	4.6	m_b (ISC)	346	3.1	76	3.6	35
74	1979.12.25	16:44:04.16	34.111	59.715	12	4.8	m_b (ISC)	340	3.1	70	3.6	35
75	1980.01.30	19:36:24.66	34.135	59.422	12	4.5	m_b (ISC)	280	2.9	10	3.1	28
76	1980.03.04	07:08:12.95	34.081	59.77	12	4.3	m_b (ISC)	342	3.7	72	4.5	53
77	1980.03.15	23:08:52.90	33.885	59.893	12	4.4	m_b (ISC)	276	3.3	6	4.3	44
78	1980.04.14	10:04:27.59	34.072	59.396	12	4.5	m_b (ISC)	33	2.9	123	3.4	31
79	1980.04.27	09:18:32.64	34.127	59.808	12	4.2	m_b (ISC)	84	4.0	174	4.6	58
80	1980.05.18	06:30:23.09	34.105	59.563	12	4.7	m_b (ISC)	304	2.7	34	3.0	25
81	1980.10.12	05:27:43.95	34.121	59.58	12	4.0	m_b (ISC)	1	3.7	91	4.9	58
82	1980.10.26	06:50:34.88	34.119	59.601	12	4.2	m_b (ISC)	347	4.1	77	4.7	59
83	1981.03.22	09:34:14.53	34.172	59.298	12	4.4	m_b (ISC)	297	3.6	27	5.0	57
84	1984.04.20	11:40:53.71	34.181	58.474	12	4.6	m_b (ISC)	270	2.8	0	3.9	34
85	1984.09.10	12:36:15.70	33.378	60.143	12	4.2	m_b (ISC)	346	4.5	76	6.4	91
86	1984.09.12	09:09:22.46	33.369	60.165	12	4.7	m_b (ISC)	87	3.7	177	4.2	48
87	1986.10.12	06:29:39.02	33.99	59.747	12	4.3	m_b (ISC)	10	3.8	100	5.9	71
88	1991.12.30	04:35:16.16	33.502	60.21	12	4.4	m_b (ISC)	302	3.3	32	3.7	37
89	1993.01.14	07:17:03.20	33.408	59.732	12	4.7	m_b (ISC)	280	2.7	10	3.8	32
90	1993.05.29	10:50:34.34	34.121	59.975	12	4.7	m_b (ISC)	304	2.8	34	3.4	30
91	1996.03.16	22:39:35.61	33.136	60.228	12	4.3	m_b (ISC)	280	2.7	10	3.9	33
92	**1997.05.10**	**07:57:30.00**	**33.88**	**59.815**	**13**	**7.2**	**M_w (HRVD, NEIC)**	**272**	**2.2**	**2**	**2.7**	**19**
93	1997.05.10	08:07:14.34	33.698	59.785	12	4.8	m_b (ISC)	39	5.4	129	10.1	171
94	1997.05.10	08:21:50.47	32.929	60.396	12	4.1	m_b (ISC)	85	5.4	175	7.1	121
95	1997.05.10	08:22:49.01	33.132	60.138	12	4.3	m_b (ISC)	51	4.7	141	5.4	80
96	1997.05.10	08:37:16.02	33.081	60.161	12	4.2	m_b (ISC)	78	5.2	168	6.5	105
97	1997.05.10	08:40:24.74	32.956	59.879	12	3.9	m_b (ISC)	47	7.8	137	12.5	306
98	1997.05.10	08:44:51.26	33.547	60.015	12	3.7	m_b (ISC)	49	5.4	139	7.8	134
99	1997.05.10	08:55:37.96	33.357	60.094	12	3.9	m_b (ISC)	53	4.3	143	6.2	83
100	1997.05.10	09:12:48.97	33.475	60.043	12	4.2	m_b (ISC)	88	2.8	178	3.8	33
101	1997.05.10	09:19:32.80	33.725	59.907	12	4.2	m_b (ISC)	89	2.5	179	3.9	31
102	1997.05.10	09:33:36.36	33.873	59.693	12	3.8	m_b (ISC)	89	5.9	179	8.1	149
103	1997.05.10	10:19:53.06	33.048	60.217	12	3.8	m_b (ISC)	58	6.8	148	8.8	190
104	1997.05.10	10:22:00.51	33.83	59.783	12	3.9	m_b (ISC)	53	5.2	143	7.5	123
105	1997.05.10	10:24:58.52	33.522	59.993	12	3.8	m_b (ISC)	55	5.4	145	7.5	128
106	1997.05.10	10:27:21.93	33.79	59.904	14	4.6	m_b (ISC)	273	2.5	3	3.3	26
107	1997.05.10	10:34:21.43	33.425	60.041	12	4.0	m_b (ISC)	270	3.3	0	5.8	60
108	1997.05.10	10:36:04.52	33.117	60.289	12	4.0	m_b (ISC)	72	6.6	162	9.1	189
109	1997.05.10	11:01:27.67	33.097	60.254	12	4.0	m_b (ISC)	272	3.3	2	5.2	54
110	1997.05.10	12:23:08.81	33.315	60.254	12	4.3	m_b (ISC)	89	2.8	179	3.8	33
111	1997.05.10	13:24:07.60	33.331	60.139	12	3.9	m_b (ISC)	83	4.0	173	5.5	69
112	1997.05.10	13:26:33.90	33.136	60.241	12	4.2	m_b (ISC)	276	3.3	6	6.9	72
113	1997.05.10	14:04:36.71	33.122	60.259	12	4.2	m_b (ISC)	273	3.2	3	4.0	39
114	1997.05.10	15:53:28.78	33.42	60.13	12	3.9	m_b (ISC)	79	4.3	169	6.1	82
115	1997.05.10	17:32:44.52	33.564	59.984	12	4.4	m_b (ISC)	78	2.7	168	3.5	30
116	1997.05.10	19:51:39.07	33.19	60.22	12	4.1	m_b (ISC)	89	3.8	179	5.0	60
117	1997.05.10	22:13:53.78	33.469	60.019	12	4.4	m_b (ISC)	89	2.5	179	3.2	25
118	1997.05.10	22:24:31.60	32.94	60.172	12	3.8	m_b (ISC)	293	4.7	23	6.2	93
119	1997.05.10	22:52:26.55	33.461	60.034	12	3.7	m_b (ISC)	271	3.1	1	4.7	47

Table 2. (*Continued.*)

No.	Date	Time (GMT)	Lat.	Long.	Dep.	Mag.	Mag. type & source	A1	L1	A2	L2	Area
120	1997.05.10	23:35:37.52	33.296	60.188	12	4.3	m_b (ISC)	277	3.0	7	3.9	36
121	1997.05.11	01:29:31.62	33.286	60.262	12	4.3	m_b (ISC)	272	2.8	2	3.9	35
122	1997.05.11	04:18:00.88	33.166	60.04	12	3.8	m_b (ISC)	286	3.4	16	5.8	61
123	1997.05.11	04:47:10.15	33.881	59.801	12	3.9	m_b (ISC)	83	3.1	173	4.6	45
124	1997.05.11	08:24:22.42	33.183	60.186	12	3.9	m_b (ISC)	277	4.4	7	5.1	70
125	1997.05.11	08:31:50.53	33.292	60.359	12	3.9	m_b (ISC)	88	3.8	178	5.4	63
126	1997.05.11	12:56:51.55	33.411	59.998	12	3.7	m_b (ISC)	46	4.7	136	8.7	129
127	1997.05.11	22:09:05.55	33.474	60.024	12	3.6	m_b (ISC)	88	2.8	178	4.1	36
128	1997.05.12	16:26:58.55	33.188	60.206	12	3.9	m_b (ISC)	90	3.2	180	4.3	44
129	1997.05.13	06:11:58.22	34.056	59.625	12	4.0	m_b (ISC)	24	3.1	114	3.7	36
130	1997.05.13	11:42:22.59	33.554	59.963	12	4.3	m_b (ISC)	289	2.6	19	3.1	26
131	1997.05.14	14:14:17.39	33.172	60.262	12	4.7	m_b (ISC)	279	2.7	9	3.6	30
132	1997.05.15	12:48:21.59	33.03	60.242	12	4.2	m_b (ISC)	312	3.0	42	3.2	29
133	1997.05.22	04:53:00.63	33.722	59.934	12	3.8	m_b (ISC)	2	3.1	92	3.2	31
134	1997.05.23	13:24:10.95	33.341	60.11	12	4.0	m_b (ISC)	53	4.7	143	7.6	111
135	1997.05.24	10:39:17.71	33.313	60.098	12	3.7	m_b (ISC)	60	4.8	150	6.9	104
136	1997.05.25	15:07:43.77	33.238	60.199	12	4.1	m_b (ISC)	282	3.0	12	3.7	35
137	1997.06.16	03:00:05.38	33.3	60.218	12	5.0	M_w (HRVD, NEIC)	276	2.3	6	3.0	22
138	1997.06.21	08:45:27.80	33.293	60.125	12	4.2	m_b (ISC)	89	2.8	179	4.5	39
139	1997.06.21	22:21:21.36	33.073	60.237	12	4.3	m_b (ISC)	277	2.6	7	3.7	31
140	1997.06.22	22:52:54.92	33.306	60.179	12	4.3	m_b (ISC)	279	2.5	9	3.6	28
141	**1997.06.25**	**19:38:41.06**	**33.972**	**59.459**	**12**	**5.9**	***M*$_w$ (HRVD, NEIC)**	**272**	**2.2**	**2**	**2.7**	**18**
142	1998.01.24	16:20:56.72	33.679	59.835	12	4.0	m_b (ISC)	278	2.7	8	3.5	30
143	1998.06.15	00:17:49.75	34.078	59.821	12	4.3	m_b (ISC)	276	2.4	6	2.9	22
144	1998.10.02	02:38:20.79	33.804	60.05	12	3.9	m_b (ISC)	305	3.7	35	4.1	48
145	1998.11.28	18:16:55.91	33.066	60.297	12	3.8	m_b (ISC)	67	6.6	157	9.4	196
146	1999.02.13	09:56:03.48	33.274	60.084	12	3.9	m_b (ISC)	285	5.0	15	9.4	147
147	2001.04.14	03:23:52.80	33.171	60.282	12	3.9	m_b (ISC)	271	3.0	1	5.2	4.2
148	2001.10.08	01:17:14.20	32.993	60.262	12	4.9	m_b (ISC)	271	2.4	1	3.0	4.9
149	2001.10.08	06:16:06.02	32.724	60.173	12	4.4	m_b (ISC)	276	2.8	6	4.3	4.3
150	2001.10.09	18:14:22.31	32.968	60.287	12	3.8	m_b (ISC)	83	3.1	173	3.8	3.9
151	2002.11.14	04:07:26.76	32.918	59.682	12	4.4	m_b (ISC)	63	2.7	153	3.2	4.6
152	2003.09.22	07:08:06.73	33.987	59.624	12	4.3	m_b (ISC)	82	2.8	172	3.4	4.3
153	2003.09.30	00:05:38.88	32.985	60.251	12	4.1	m_b (ISC)	65	3.3	155	4.4	4.1
154	2003.11.16	22:51:34.81	33.314	60.129	12	4.7	m_b (ISC)	86	2.2	176	2.7	4.8
155	2003.11.16	23:34:05.70	33.321	60.151	12	4.1	m_b (ISC)	75	2.5	165	3.2	4.3
156	2005.12.27	08:37:15.23	33.459	60.069	12	3.9	m_b (ISC)	69	2.7	159	3.8	4
157	2005.12.27	11:06:21.59	33.553	59.901	12	3.7	M_L (CSEM)	36	3.3	126	7.6	3.7
158	2006.07.16	21:31:19.32	33.509	60.009	12	3.7	M_L (CSEM)	34	3.0	124	8.5	3.7
159	2006.09.11	14:01:16.46	33.08	60.287	12	4.4	m_b (ISC)	81	2.3	171	2.8	4.4
160	2006.11.13	04:56:25.45	34.029	59.778	12	3.7	M_L (CSEM)	22	3.0	112	4.5	3.7
161	2007.01.22	05:13:11.72	33.45	59.273	12	3.5	M_L (CSEM)	11	2.6	101	3.3	3.5
162	2007.03.13	15:35:02.93	33.223	60.179	12	3.5	m_b (ISC)	47	2.6	137	3.5	3.6
163	2007.08.15	21:58:09.38	33.442	60.053	12	3.6	M_L (CSEM)	36	2.7	126	4.5	3.6
164	2008.03.09	03:51:05.59	33.255	59.253	12	5.0	M_w (GCMT)	86	2.5	176	2.7	5
165	2008.03.09	09:43:42.07	33.27	59.148	12	3.4	m_b (ISC)	1	3.3	91	6.2	3.4
166	2008.06.27	14:58:16.67	33.46	59.058	12	3.7	m_b (ISC)	287	4.5	17	4.8	4
167	2008.09.23	04:34:03.22	32.982	60.311	12	3.8	m_b (ISC)	60	2.9	150	3.7	4.2
168	2008.11.18	11:20:37.91	33.28	59.129	12	3.6	m_b (ISC)	62	4.7	152	5.9	4.2
169	2008.12.24	19:49:03.88	32.658	59.406	12	3.6	M_L (CSEM)	52	2.7	142	3.9	3.6

described in Section 4. Maps of the first five of these subclusters are shown in Fig. 6. The last two are shown in Fig. 10.

4 MAJOR SEQUENCES THROUGH TIME

In this section, we review the seismicity of the study region chronologically, divided into several major sequences of seismic activity and the intersequence periods (Table 3). In discussing individual earthquakes, we will usually reference the date and also the event number as listed in Table 2.

4.1 Dasht-e-Bayaz sequence

The 1968 August 30 Dasht-e-Bayaz earthquake (#5, M_w 7.1) caused widespread destruction, killing between 7000 and 12 000 people, and making at least 70 000 homeless. The earthquake produced ∼80 km of surface ruptures along the Dasht-e-Bayaz Fault from longitude ∼58°35′E to east of Zigan village (longitude 59°25′; see Fig. 6a). The average left-lateral displacement was estimated at ∼2 m, though maximum left-lateral displacements of ∼4.5 m and vertical displacements of ∼2.5 m were observed (Ambraseys & Tchalenko 1969). Our calibrated relocation shifts the epicentre about 4 km from the single-event location of Engdahl *et al.* (1998),

Table 3. Summary of the seven chronological divisions used to separate the earthquakes listed in Table 2 into the main sequences.

Sequence	Date range	Event No.	Figure
Dasht-e-Bayaz	1968/08/31 – 1968/11/28	5–25	Fig. 6(a)
Intersequence 1	1969/08/23 – 1979/08/25	26–46	Fig. 6(b)
Korizon	1979/11/14 – 1979/11/27	47–54	Fig. 6(c)
Koli-Buniabad	1979/11/27 – 1979/12/25	55–74	Fig. 6(d)
Intersequence 2	1980/01/30 – 1996/03/16	75–91	Fig. 6(e)
Zirkuh	1997/05/10 – 1997/06/25	92–141	Fig. 10(a)
Intersequence 3	1998/01/24 – 2008/12/24	142–169	Fig. 10(b)

but does not change the conclusion that the earthquake is likely to have nucleated at a prominent extensional segment boundary near the eastern margin of the Nimbluk Valley, as suggested by Walker *et al.* (2004).

Our relocated cluster includes 20 aftershocks of the Dasht-e-Bayaz earthquake, continuing for 3 months until late November and followed by a 9-month gap until the next event in the cluster (Table 3). The locations of the aftershocks are shown in Fig. 6(a). Three notable aftershocks occurred in the days following the 1968 Dasht-e-Bayaz earthquake. Two of these, the September 1 and 4 Ferdows earthquakes (#9 and 17 in Table 2), occurred on a northwest–southeast trending thrust fault on the west side of the Kuh-e-Siah range, 30 or more kilometres west of the mapped surface faulting for the main shock (Fig. 6a). The third event (1968 September 11, #20, M_w 5.6) is located right on the Dasht-e-Bayaz fault trace (Fig. 6a, also see Fig. 15). Its position, ∼4 km east of Zigan village, is at the eastern end of the main shock rupture.

Other aftershocks, both early and late, on the eastern end of the main faulting trace are located a few kilometres to the north, on a NE–SW trend, which reflects the trend of several mapped fault strands in the area (as shown in Fig. 6a). Aftershocks are concentrated in two places, the eastern end of the rupture zone and on the western side of the Kuh-e Siah range, near Ferdows (Fig. 6a), well beyond the western limit of coseismic faulting.

The earthquakes near Ferdows are considered in more detail later. We suggest that the pattern of aftershock seismicity in the eastern part of the rupture might also reveal the presence of additional active structures north of the main Dasht-e-Bayaz trace (Fig. 6a). We note that a subevent of the Dasht-e-Bayaz earthquake, placed ∼24 km east of the main shock epicentre, and involving reverse slip on a northwest–southeast plane was required to fit some details of the body waveforms (Walker *et al.* 2004). This subevent, though not precisely located, will have occurred somewhere to the northeast of the mountainous Kuh-e-Meykay region where thrust faulting on the same northwest–southeast orientation is visible in the geomorphology (as marked on Fig. 6a).

There are also several aftershocks (1968 September 1, #11, m_b 4.9 and 1968 November 28, #25, m_b 4.8) east of the main shock rupture zone, near the intersection of the Dasht-e-Bayaz and Abiz faults. This later event should perhaps not be considered part of the Dasht-e-Bayaz aftershock sequence.

4.2 Intersequence: between the Dasht-e-Bayaz and Korizan sequences

Between the end of the 1968 Dasht-e-Bayaz aftershock sequence in late 1968 and the onset of rupture in a series of large events on the eastern end of the Dasht-e-Bayaz fault in late 1979, seismicity falls mainly into three categories: (1) continued faulting in places that were seismically active in the 1968 Dasht-e-Bayaz aftershock sequence, including the Ferdows region, (2) faulting in 1976 north of the city of Qayen and south of the Dasht-e-Bayaz Fault and (3) the Boznabad main shock–aftershock sequence near the eastern Dasht-e-Bayaz Fault in early 1979 (Fig. 6b).

The 1976 November 7 earthquake (#32, M_w 6.0) occurred in the sparsely populated region north of Qayen. The town has been damaged by a number of historical earthquakes including events in 1066 and 1847 AD (e.g. Ambraseys & Melville 1982; Berberian & Yeats 1999; Berberian & Yeats 2001; Walker *et al.* 2004). None of the historical events are tied to individual faults. A number of faults are visible near Qayen in satellite imagery. These include a band of E–W faulting ∼10 km to the north, a series of NW–SE scarps cutting alluvial fan deposits a similar distance to the west and several N–S trending faults east of the town (Figs 5 and7).

Berberian *et al.* (1999), tentatively attributed the 1976 November 7 earthquake to the E–W Avash Fault, which runs through the Kuh-e-Avash mountains north of Qayen, and on which they identify late Quaternary left-lateral stream displacements. Our relocation of the 1976 main shock, and two subsequent events (1976 November 9, #33, m_b 5.1 and 1977 March 19, #34, m_b 4.7), provide strong support for slip on the Avash Fault as the cause of the events (Fig. 7). We cannot verify the existence of recent displacements along the Avash Fault within the Kuh-e-Avash mountains. However, where segments of the fault run through the alluvial fans at the southern margin of the Nimbluk Valley there are signs of late Quaternary activity. In Fig. 8, we show two close-up satellite images with indications of active faulting. In the first, a linear scarp with a low north-facing scarp cuts across alluvial fans. In the second, a fault cuts through an incised alluvial fan and left-laterally displaces the stream channels.

On 1979 January 16, a large earthquake (#36, M_w 6.5) occurred about 6 km south of the eastern part of the Dasht-e-Bayaz Fault (Fig. 6b). We refer to this as the Boznabad earthquake after a nearby village. This sequence is discussed further in Section 5.3.

4.3 Korizan sequence

On 1979 November 14, a remarkable sequence of major earthquakes on the eastern end of the Dasht-e-Bayaz Fault initiated with the Korizan earthquake (#47, M_w 6.8, Fig. 6c). The earthquake killed 171 people, injured 297 and produced 20 km of surface ruptures along the northern Abiz Fault from south of Estend to near the Kal-e-Shur River (Haghipour & Amidi 1980; Fig. 9). A maximum right-lateral displacement of 100 cm was observed at Korizan. A large vertical component of displacement was mapped in the bed of a dry stream 2 km north of Korizan. The earthquake destroyed the villages of Korizan, Niar Estend, Bohnabas and Fandokht. It also destroyed the villages of Garmab and Tighab, which are sited along the western margin of Shahaz Kuh (Fig. 9).

The calibrated main shock epicentre is situated several kilometres west of the Abiz Fault, which might explain the destruction of Garmab and Tighan villages. Body-waveform modelling of the Korizan earthquake indicates that it was a multiple event with two pure right-lateral subevents, the first striking 160° (shown in Fig. 9) and the second 175°, consistent with the arcuate fault trace, but inconsistent with the epicentral location of the main shock at the northern end of the surface rupture. A southward rupture propagation would result in a change from roughly N–S faulting to a trend of ∼160°, opposite to the change modelled from body waveforms (Berberian *et al.* 1999).

The aftershock sequence (Fig. 6c) can be clearly observed for 2 weeks (events #48–54) until the Khuli-Buniabad main shock on

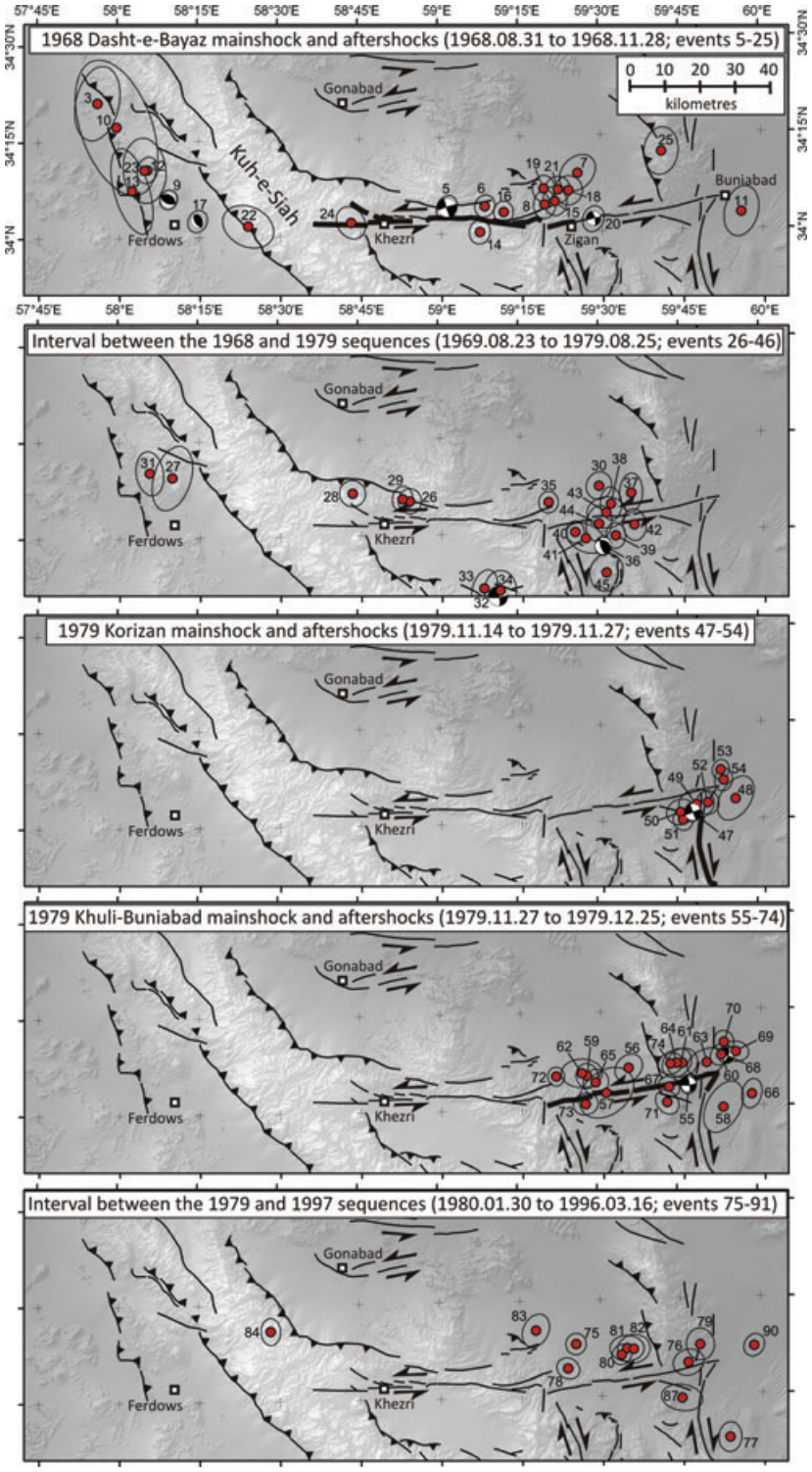

Figure 6. (a) Epicentre of the 1968 August 31 M_w 7.1 Dasht-e-Bayaz main shock (event 5) and aftershocks over the following 3 months. Thickened black lines show the extent of surface rupturing in the main shock. The most notable aftershocks were the 1968 September 1 and 4 Ferdows earthquakes (#9, M_w 6.3 and #17, M_w 5.5) beyond the western end of the main shock rupture and the 1968 September 11 (#20, M_w 5.6) event near the eastern end. (b) Seismicity recorded in the decade between the 1968 Dasht-e-Bayaz and 1979 Korizan earthquake sequences. This period includes the 1976 November 7 Qayen main shock (#32, M_w 6.0) and the 1979 January 16 Boznabad earthquake (#36, M_w 6.5). (c) Main shock and aftershock sequence of the 1979 November 14 Korizan earthquake (#47, M_w 6.6). The seismicity in this panel occurred over a time period of only 2 weeks. The mapped rupture, which involved right-lateral slip on the N–S Abiz Fault, continued south of the region shown in this map. (d) Main shock and aftershocks of the 1979 November 27 Khuli-Buniabad earthquake (#55, M_w 7.1). The most prominent aftershock in this sequence is the 1979 December 7 Kalat-e-Shur event (#68, M_w 5.9). Slip in the Khuli-Buniabad main shock generated surface rupture along the eastern half of the Dasht-e-Bayaz Fault (apparently including a re-rupture of part of the section that broke in 1968). Our analysis of epicentral locations favours the Khuli-Buniabad earthquake as the source of ∼10 km of N–S right-lateral rupture at the northern end of the Abiz Fault. See Fig. 5 for location.

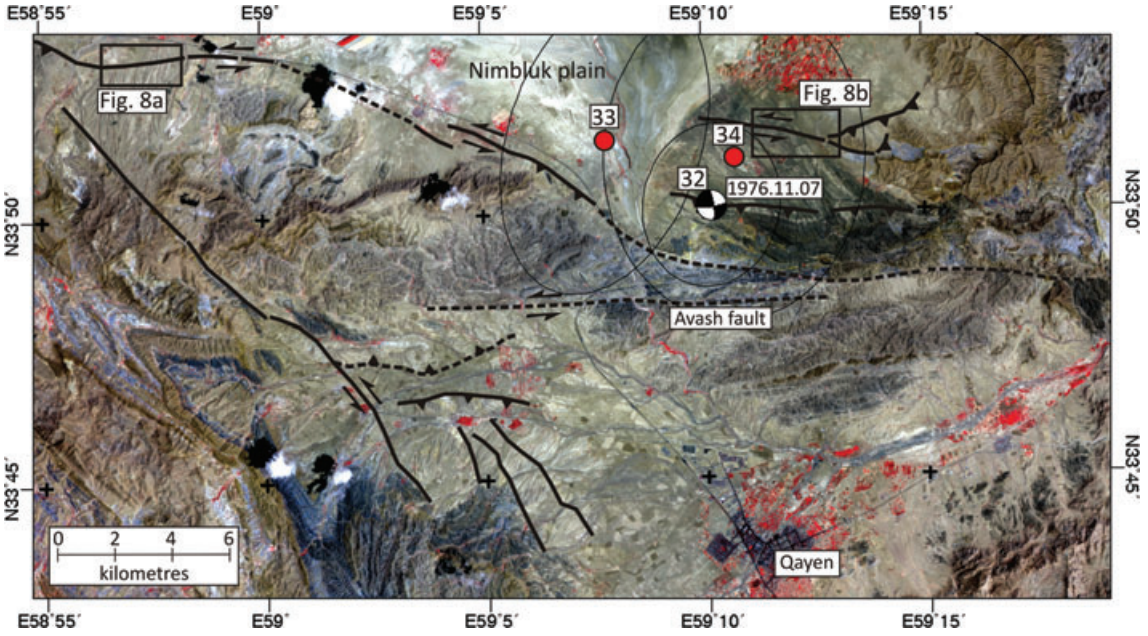

Figure 7. ASTER satellite image (RGB, 321) of the 1976 November 7 Qayen earthquake (#32, M_w 6.0) epicentral region (see Fig. 1c for location). The E–W Avash Fault (e.g. Berberian *et al.* 1999; Berberian & Yeats 2001) runs through the narrow band of mountains that separate the Nimbluk plain in the north from the Qayen plain to the south. Late Quaternary scarps, showing oblique left-lateral and reverse slip, are visible on fault segments at the margin of the Nimbluk plain (see Fig. 8 for close-up views of these scarps). The fault responsible for these scarps is unnamed. The epicentres of the 1976 main shock and of two smaller events are situated along the southern edge of the Nimbluk plain. We suggest that they occurred on the late Quaternary faults running along the edge of the plain.

November 27. The epicentres of the main shock and its aftershocks show an alignment on an NE–SW trend that roughly divides the E–W Dasht-e-Bayaz Fault and the N–S Abiz Fault. The siting of the main shock epicentre west of the surface rupture, the multiple-event source and the NE–SW alignment of aftershock activity all suggest that the Korizan earthquake may have included an initial subevent on a fault west of the main Abiz Fault.

The two latest aftershocks (1979 November 23, #53, m_b 5.0 and 1979 November 27, #54, m_b 5.1) are located a few kilometres north of the intersection of the Dasht-e-Bayaz and Abiz faults. Because of the gap in time between these events and the immediate aftershocks of the Korizan main shock, these two events should perhaps be seen as precursors to the Khuli-Buniabad main shock. We also note that these two events are located exactly where the Kalat-e-Shur event will occur a few weeks later (see below).

4.4 Khuli-Buniabad sequence

The 1979 November 27 Khuli-Buniabad earthquake (M_w 7.1) produced ∼60 km of surface ruptures along the eastern part of the Dasht-e-Bayaz Fault, from west of Zigan village in the west to Buniabad in the east (Fig. 6d). The earthquake apparently re-ruptured the eastern ∼10 km of the surface breaks generated during the 1968 Dasht-e-Bayaz earthquake, which extended east of the village of Zigan (Ambraseys & Tchalenko 1969). The relocated epicentre of this earthquake agrees with the existing interpretation of a westward-propagating rupture, which may have contributed to rupture propagation into the zone previously ruptured in 1968.

Aftershock activity lasted about a month, until the end of 1979 December, and it is distributed fairly evenly along the full E–W extent of main shock rupture. The majority of the aftershocks are located to the north of the Dasht-e-Bayaz Fault, consistent with a slight northward dip on the fault plane, as seen in the source parameters of both the Dasht-e-Bayaz and Khuli-Buniabad main shocks (Walker *et al.* 2004). Uplift of the north side of the Dasht-e-Bayaz Fault is also apparent from the pattern of drainage incision (Walker *et al.* 2004).

Among the aftershocks of the Khuli-Buniabad event was a large (#68, M_w 5.9) event on 1979 December 7, known as the Kalat-e-Shur event. This event is discussed further in Section 5.4.

4.5 Intersequence: between Khuli-Buniabad and Zirkuh sequences

The 16-year period between the end of major aftershock activity related to the 1979 Khuli-Buniabad event and the 1997 Zirkuh sequence contains no events as large as magnitude 5.0, and the pattern of seismicity is diffuse (Fig. 6e). Most of the activity is associated with deformation as much as 15 km north of the Dasht-e-Bayaz Fault, along the section that ruptured in the Khuli-Buniabad event, and can be considered as an extended aftershock sequence. There is a suggestion of deformation migrating slowly northward from the Dasht-e-Bayaz Fault. Note that a small number of events during this period in the southeastern part of the study area are not covered by Fig. 6(e).

4.6 Zirkuh sequence

The M_w 7.1 Zirkuh earthquake occurred on 1997 May 10 at 12:28 p.m. local time. Over 1500 people were killed, a further 2600 injured, 12 000 houses destroyed and 7000 more were damaged (Berberian *et al.* 1999). It produced ∼125 km of surface rupture on the Abiz Fault from its junction with the E–W Dasht-e-Bayaz Fault in the north to Sepestan Mountain in the south (Ikeda *et al.* 1998; Berberian *et al.* 1999; Fig. 10a). It re-ruptured the parts of the northern

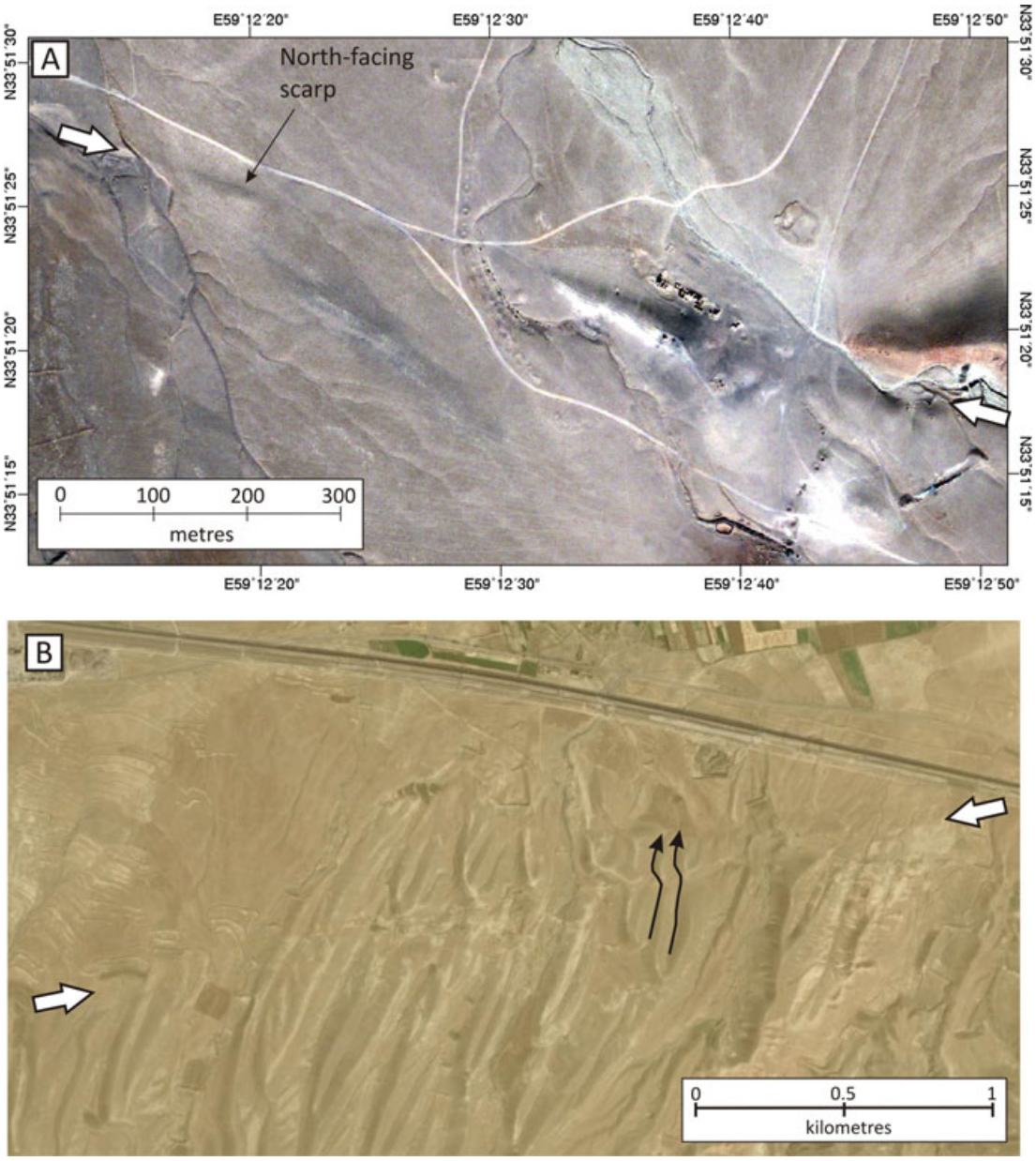

Figure 8. Close-up views of active faulting along the southern margin of the Nimbluk plain. (a) Pan-sharpened IKONOS image of a linear, late Quaternary, fault trace running between the white arrows. A vertical component forming a low north-facing scarp is labelled particularly apparent in the left half of the image where the fault cuts across a wide alluvial fan surface. (b) Left-lateral displacement of incised fan surface just south to the Qayen to Gonabad highway (SPOT5 imagery from Google Earth). The channels of two of the incised drainage channels have been highlighted in black. Left-lateral displacement of several tens of metres is visible at the fault trace.

Abiz Fault that had also failed during the complex sequence of earthquakes in 1979. It also re-ruptured a section of fault that had failed in the 1936 June 30 (M_s 6.0) Abiz earthquake. The coseismic ruptures were predominantly right-lateral strike-slip, with typical horizontal slip of 80–140 cm and a maximum horizontal displacement of 230 cm. Vertical displacements of up to 90 cm were also measured (Berberian *et al.* 1999). Body wave modelling of the Zirkuh earthquake indicates a complex rupture with at least four subevents (Berberian *et al.* 1999). A complex rupture is also suggested from a source model derived from InSAR that indicates variable dip and rake along the fault, and with three main rupture sections separated by regions of low slip at Bohnabad and a few kilometres south of Ardekul (Sudhaus & Jónsson 2011). The InSAR model also shows an apparent slip deficit at the surface, with a modelled peak slip of 4 m beneath Ardekul. The aftershock sequence was very active, extending into late 1997 June and including events 93–141 of our relocated data set.

As part of the indirect calibration process for locations, we constrained the epicentre of the Zirkuh main shock to be at the longitude of the mapped rupture (latitude was constrained by the Dasht-e-Bayaz and Khuli-Buniabad epicentres). The calibrated location of the main shock epicentre is at the northern margin of Shaskuh Mountain (Fig. 9), and none of the relocated aftershocks occurred on the Abiz Fault north of this point. The relocated epicentres of the 1997 Zirkuh aftershock sequence show a strong correlation with the mapped trace of the main shock rupture to the south of

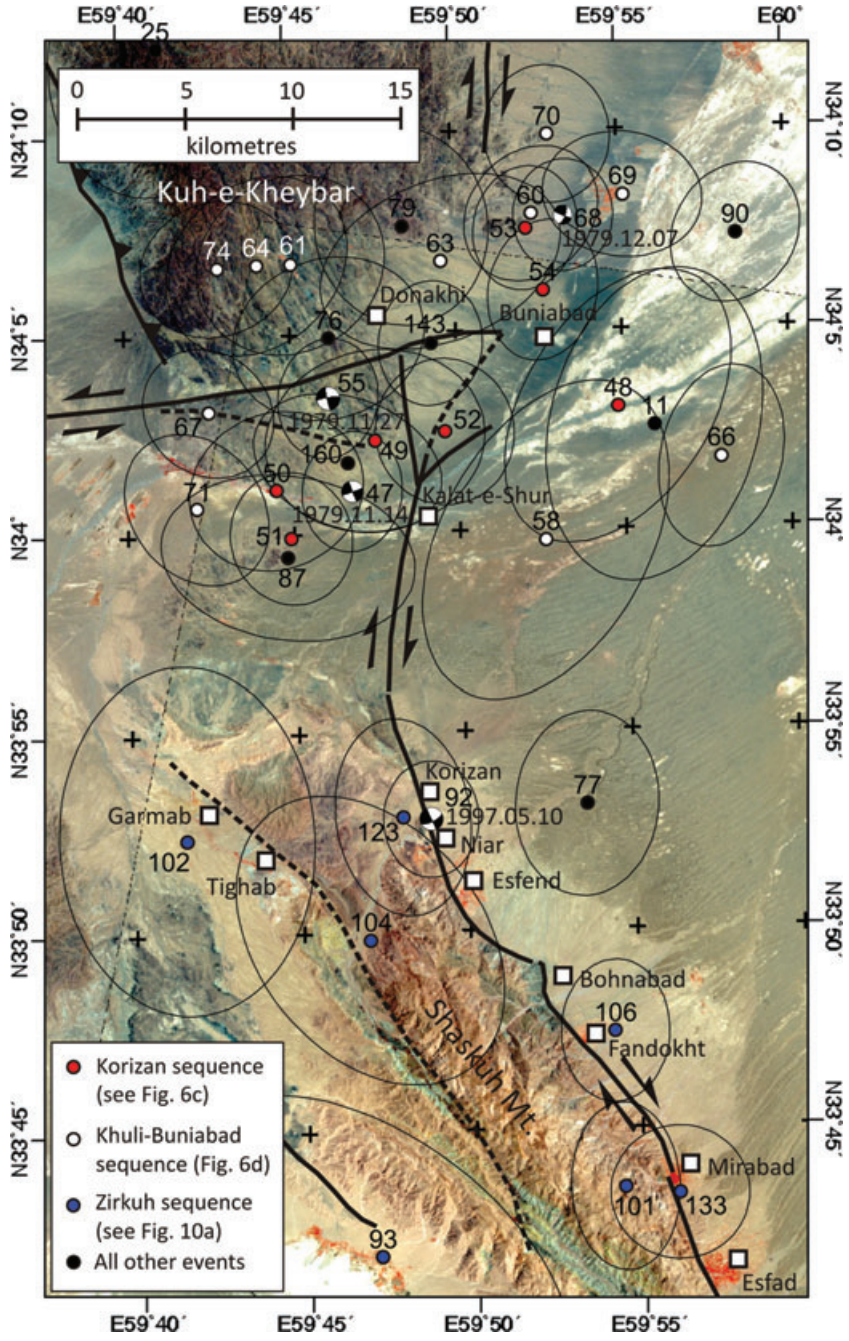

Figure 9. LANDSAT satellite image (RGB bands 421) of the northern Abiz Fault and surroundings (see Fig. 1c for location). The 1979 November 14 M_w 6.6 Korizan earthquake (#47) ruptured the surface from just south of Esfad to Kalat-e-Shur. Its epicentre at the northern end of these surface breaks shows southward rupture propagation. The right-lateral ruptures extending from Kalat-e-Shur to Donakhi are attributed either to a subevent of the 1979 November 27 M_w 7.1 Khuli-Buniabad earthquake (#55) or to slip in the 1979 December 7 M_w 5.9 Kalat-e-Shur earthquake (#68). The calibrated epicentre of the Kalat-e-Shur earthquake is situated ∼10 km northeast of Donakhi, and is separated from the ruptures by the active trace of the Dasht-e-Bayaz Fault. We suggest that the 1979 December 7 earthquake was instead associated with rupture of N–S faults along the eastern margin of Kuh-e-Kheybar (see Section 5.4). In that case, the ruptures from Kalat-e-Shur to Donakhi are likely to be a subsidiary rupture of the 1979 November 27 Khuli-Buniabad earthquake.

the epicentre (Fig. 10). The largest concentration of aftershock activity is found in the southern part of the rupture zone, starting 35–40 km south of the epicentre, southward from the village of Hajiabad, in a region in which the fault runs through high mountainous topography (Fig. 11). Within this southern section, the seismicity expresses clustering immediately south of Hajjiabad (between latitudes 33°25′N and 33°30′N, see Fig. 11), adjacent to Ahangaran Mountain (at latitude 33°15′N to 33°20′N), and around Sepestan Mountain (near latitude 33°05′N). The three clusters of epicentres are coincident with the intersection of the main Abiz Fault with E–W to ESE–WNW trending faults that branch from both its eastern and western sides (Fig. 11) and an E–W alignment in seismicity is apparent in the central cluster (between the white arrows in Fig. 11). We suspect that the increased density of aftershock activity in these

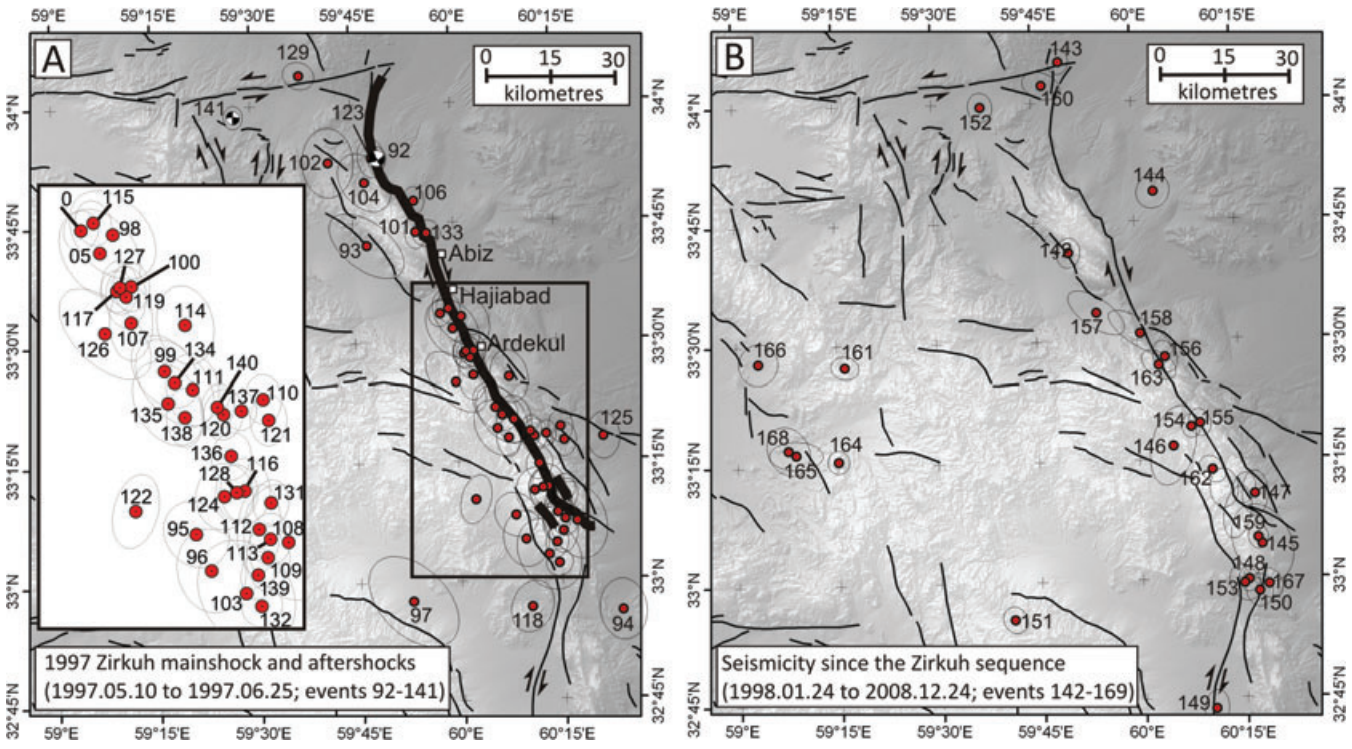

Figure 10. (a) Main shock and aftershocks of the 1997 May 10 M_w 7.2 Zirkuh earthquake (#92). The earthquake generated ∼120 km of predominantly right-lateral surface ruptures (shown as thickened black lines) along the N–S Abiz Fault. The most prominent aftershock is the 1997 June 25 Boznabad event (#141, M_w 5.9) which occurred well away from the main zone of rupture. (b) Epicentres of earthquakes occurring in the years following the 1997 Zirkuh sequence. Additional seismicity continued in the vicinity of the Abiz Fault as well as scattered activity in the southwestern part of the region of study. See Fig. 5 for location.

regions represent structural complexity at the intersection between the E–W faults and the main Abiz Fault. The E–W faults have a component of dip-slip that is visible as scarps in Quaternary alluvium (Fig. 11). We also suspect that they possess a component of left-lateral strike-slip: apparent left-lateral displacement of distinctive dark-coloured bedrock units across two of the E–W faults are highlighted on Fig. 11.

Discontinuous N–S to NNE–SSW trending ruptures (with up to 15 cm of right-lateral displacement) were found in the desiccated lake basins of Avaz and Nasr al-Din villages ∼20 km south of the end of the main Abiz Fault (Berberian *et al.* 1999). Although a number of epicentres are located south of the end of the 1997 rupture near the villages of Gazik and Avaz (Fig. 11) they mainly occurred after the main aftershock sequence and do not extend far enough to the south to be responsible for this southern zone of ground rupturing.

4.7 Seismicity since the Zirkuh sequence

After late 1997 June, the next event in the region that is well enough recorded to be relocated occurs in 1998 January. Seismicity in the following 10 years is diffuse and of low magnitude, the largest event having a magnitude of 5.0 M_w (2008 March 9, #164, Fig. 10b). Most of the seismicity can be considered aftershocks of the 1997 Zirkuh event, occurring mainly in the southern half of the rupture zone where the immediate aftershock activity also was concentrated. A few events appear to be related to the rupture zones of the Khuli-Buniabad and Korizan events, and there is a small group of events in the remote mountainous region that forms the western part of the study region. This western region is discussed in Section 5.1.

5 EARTHQUAKES OF INTEREST

In this section, we look in more detail at some of the earthquakes discussed earlier in the context of larger sequences. Each of the sections focuses on one part of the larger earthquake sequence in which the faulting is not well understood and in which the calibrated epicentres, along with an analysis of satellite imagery and of ground deformation imaged by InSAR in one case, helps to constrain the earthquake source.

5.1 The 1947 Dustabad earthquake and seismicity in the SW of the study region

The 1947 September 23 Dustabad earthquake (M_s 6.8, #1) is the earliest event to be included in our relocation analysis. It occurred within a sparsely populated desert region north of the Daqq-e-Muhammadabad (a flat, salt-encrusted and internally drained basin) in which several N–S right-lateral faults are mapped (Fig. 12). The Dustabad earthquake was the second of three 20th century earthquakes known within this desert region (e.g. Ambraseys & Melville 1982). The first, on 1941 February 16, killed 680 people and is likely to have ruptured the northern ∼10 km of the Chahak Fault (Fig. 12). The arrival time data for this event were inadequate to usefully constrain the location in our relocation study. A third earthquake, on 1962 April 1 (M_s 5.8, #2), has a calibrated epicentre lying right on the Chahak Fault (Fig. 12). The damage distribution from this earthquake suggests that it is likely to have occurred on the southern part of the Chahak Fault (Ambraseys & Melville 1982) and we hence suspect that it propagated southwards from the southern end of the 1941 rupture.

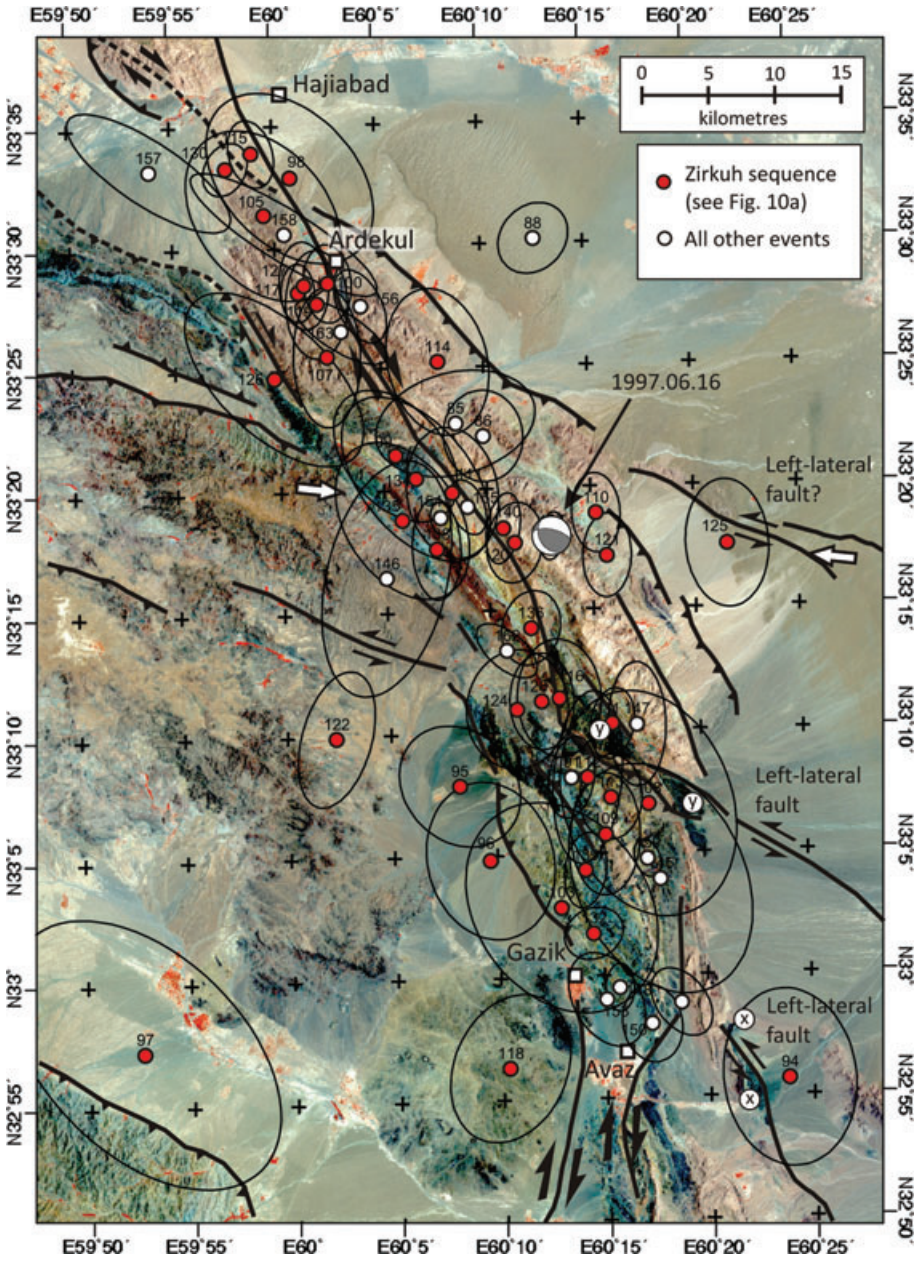

Figure 11. LANDSAT image (RGB bands 421) showing events along the southern part of the Abiz Fault (see Fig. 1c for location). Aftershocks of the 1997 Zirkuh earthquake are shown in red. Other events are in white. Ninety per cent confidence ellipses are for cluster vectors alone. A possible clustering of events is seen at two places where the N–S Abiz Fault intersects with E–W structures. The E–W structures may possess a component of left-lateral slip, as is suggested from the apparent left-lateral displacement of dark-coloured lithologies across them at points marked X and Y. An E–W alignment in epicentres is apparent in the northern cluster (between the white arrows).

The calibrated location of the 1947 Dustabad earthquake, which places the event in the remote Kuh-e-Shekasteh region (Fig. 12), is rather surprising given that Ambraseys & Melville (1982) report ∼20 km of ruptures from this earthquake along the Dustabad Fault, roughly 20 km to the east of the calibrated epicentre (Fig. 12). The eroded ruptures, to which Ambraseys & Melville (1982) were guided in 1978, consisted of a series of discontinuous cracks, trending ∼350°, with right-lateral offsets of ∼1 m and vertical offsets of 30–80 cm visible at some locations. Local information suggested that ground deformation continued northwards across the alluvial plains to the village of Ishtakhr (Fig. 12). It is unlikely that the field observations, which were detailed and refer to known geographical locations, are incorrect—though they were visited 30 years after the event and a possibility remains that the association of the eroded ruptures at Dustabad with the 1947 is erroneous.

We have a high degree of confidence in the relocated epicentre of this event, especially given the very close correlation between all the other relocated epicentres and active faults, including mapped surface ruptures in several cases. Nevertheless, we carried out several studies to investigate if the event could have occurred on the Dustabad Fault. One such test is to carry out the relocation of the cluster with the 1947 event's epicentre fixed on the Dustabad Fault (origin time is the only free parameter). We found that such a location violated an unusually large percentage of the reported arrival time data. We also examined the arrival time data for the event carefully. Because multiple-event relocation relies on traveltime

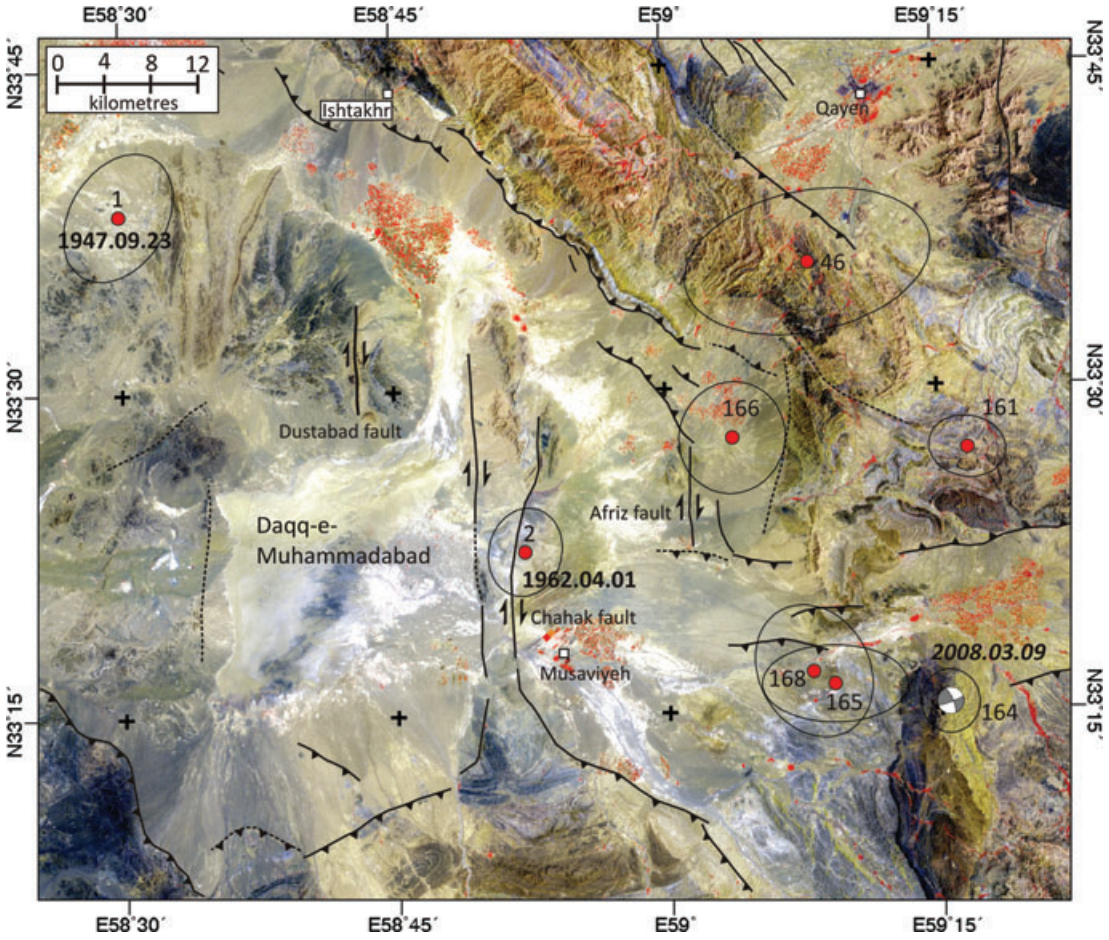

Figure 12. ASTER satellite image (RGB, 321) of the SW part of our study region (see Fig. 1c for location). The northwest–southeast trending Ferdows thrust is visible in the top right of the image. The epicentre of the 1947 September 23 earthquake (#1, M_S 6.8) is situated in a remote region of low mountains with N–S aligned bedrock exposure. Ambraseys & Melville (1982) report eroded surface ruptures of the 1947 earthquake ∼15 km southeast of the epicentre along the Dustabad Fault. The 1962 April 1 Musaviyeh earthquake (#2, M_S 5.8) is located right on the Chahak Fault. This earthquake is thought to have ruptured the southern part of the Chahak Fault (Ambraseys & Melville 1982) implying southward propagation of rupture during this event. An earthquake on 1941 February 16, which is not included in our catalogue of events, is thought to have ruptured the northern 10 km of the Chahak Fault (Ambraseys & Melville 1982).

differences, the only readings that have any influence on the 1947 event's location are those that have 'connectivity' for the cluster vector (i.e. there are other observations of the same phase at the same station for other events in the cluster). There are only three such readings in the Southern Hemisphere at epicentral distances less than 100°, *P* arrivals at KOD (Kodaikanal, India) ($\Delta = 29.1°$) and BOM (Mumbai, India) ($\Delta = 19.5°$) and a Pn reading at NDI (New Delhi, India) ($\Delta = 17.8°$). All three are in the southeast quadrant (azimuth 102°–139°), in the direction that the epicentre would need to shift to have a location on the Dustabad Fault. These readings therefore have a strong influence on the question of whether a location on the Dustabad Fault can be consistent with the seismic data. The *P* arrivals at BOM and KOD are consistent with each other, but not with the Pn arrival at NDI, which is relatively early (i.e. it would prefer a location closer to the Dustabad Fault). Our preferred location relies on BOM and KOD and flags the NDI arrival as an outlier. If we flag the BOM and KOD readings as outliers and fit the NDI reading the location shifts 10 km southeast (33.515°N, 58.575°E) but it is still about 12 km west of the Dustabad Fault, which is well outside the 90 per cent confidence ellipse for the epicentre. We investigated if this location brings any other readings that had been flagged as outliers into agreement, but there are none. The precisions of the locations, as measured by the confidence ellipses, are similar. Clearly, the uncertainty in the seismological location of the 1947 event is more uncertain than the formal errors, because of the small number of (mutually inconsistent) readings that control the location. However, neither of the locations we tested is compatible with a location on the Dustabad Fault. It is unlikely, given the event's age and the weakness of the seismic data, that the discrepancy between the epicentral location for the 1947 earthquake and the surface ruptures attributed to it will be easily resolved.

Several other faults in the vicinity of the Daqq-e-Muhammadabad are associated with scattered seismicity (Fig. 12). Six events are located east of the Afriz Fault in a region of scattered, and somewhat complex, faulting involving N–S right-lateral, E–W left-lateral and NW–SE thrusting. The largest of these events (2008 March 9, #164, M_w 5.0), has a Harvard CMT solution showing either E–W left-lateral, or N–S right-lateral, faulting. Given the close proximity of this event to both E–W and N–S faults we cannot distinguish which of the nodal planes represents the fault orientation.

5.2 The 1968 September 1 and 4 Ferdows earthquakes

During the aftershock sequence of the 1968 Dasht-e-Bayaz earthquake, two destructive earthquakes (1968 September 1, #9, M_w 6.3 and 1968 September 4, #17, M_w 5.5) occurred significantly west

of the main shock rupture zone (Fig. 6a), killing ∼900 people and badly damaging the town of Ferdows and surroundings villages (Ambraseys & Melville 1982). We relocated four other events in this area, which should probably be considered as aftershocks of the first Ferdows event. The source parameters of both earthquakes indicate slip on a fault trending NW–SE to NNW–SSE, dipping ∼35° to the NE, and with centroid depths of 9–10 km (Fig. 13; Table 1). Walker *et al.* (2003) suggest that the two earthquakes occurred on the Ferdows thrust fault (Fig. 13), which has a prominent expression in the geomorphology—showing that it has been active in the late Quaternary, and which has an appropriate strike direction of ∼320° (Fig. 13). Possible surface ruptures were reported within folded Neogene sediments in the uplifted hangingwall of the fault. The ruptures were not, however, investigated by reliable observers at the time (Jackson & Fitch 1979; Ambraseys & Melville 1982).

The single-event epicentres of the Ferdows earthquakes, done with a standard, uncalibrated teleseismic location method (Engdahl *et al.* 1998), are sited ∼15 km southwest of the surface trace of the Ferdows Fault (Walker *et al.* 2003). Given that the fault is a thrust dipping to the northeast, and that the earthquakes had centroid depths of ∼10 km, the true epicentres should be located

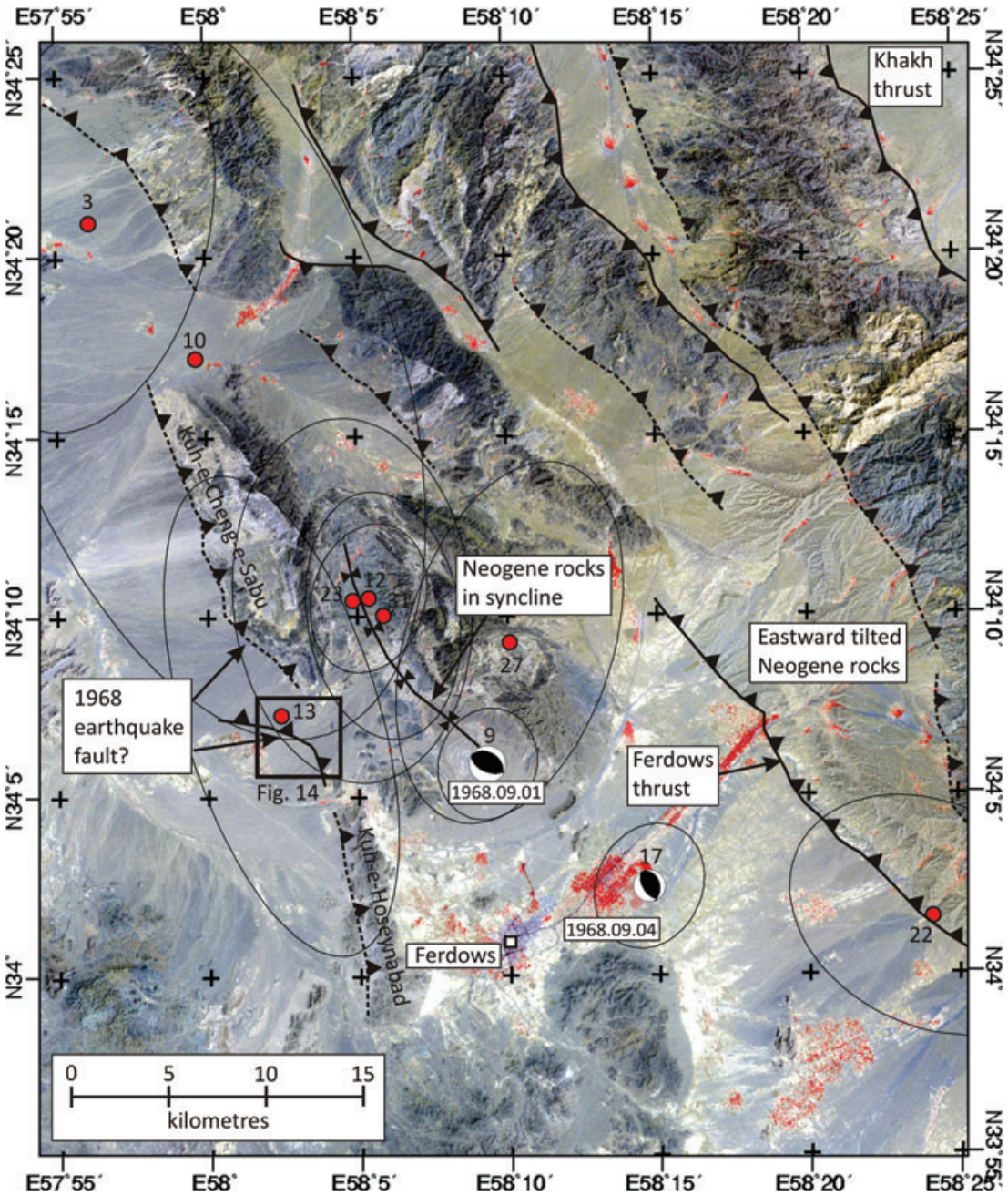

Figure 13. LANDSAT satellite image (RGB bands 421) showing the region around Ferdows (see Fig. 1c for location). The two Ferdows earthquakes of 1968 September 1 and 4 (#9, M_w 6.3 and #17, M_w 5.5) have previously been associated with the NE-dipping Ferdows thrust that exposes eastward-tilted Neogene rocks in its hangingwall. Our epicentres for the two events show that they occurred ∼10 km into the footwall of the Ferdows thrust. We suggest that the earthquakes are likely to have occurred on a newly identified thrust fault that comes to the surface in the desert regions ∼15 km northwest of Ferdows (see Fig. 14). Neogene rocks are folded into a syncline east of the newly identified fault north of Ferdows.

several kilometres northeast of the fault trace. Walker *et al.* (2003) suggested that location bias introduced by departures from a homogeneously layered Earth, which may cause offset of teleseismic epicentres from their true position by up to ∼10 km (e.g. Berberian 1979) could explain the apparent mislocation of the Ferdows events in the footwall of the Ferdows thrust fault. However, our calibrated relocations (Fig. 13) show that the two Ferdows earthquakes, along with their aftershocks, all occurred at distances of at least 10 km into the footwall of the Ferdows thrust. Rupture of the Ferdows thrust is therefore extremely unlikely to have generated the destructive Ferdows earthquakes in 1968 September.

Analysis of IKONOS satellite imagery shows a subtle scarp crossing alluvial fan deposits in the remote desert regions ∼15 km northwest of Ferdows that is an alternative, and, given the calibrated epicentral locations, more likely source of the 1968 Ferdows earthquakes (Figs 13 and 14). The alluvial fans are uplifted and incised on the northeastern side of the scarp, which places the epicentres of the Ferdows earthquakes within its hangingwall. This fault scarp has not been visited in the field. Fresh scarps are not visible in the river channels (Fig. 14, inset) and it is likely that, if slip in the Ferdows earthquakes reached the Earth's surface along this fault line, that evidence for it might already be obliterated by erosion.

The west-facing scarp in alluvium shown in Fig. 13 strikes northward towards the western margin of Kuh-e-Cheng-e-Sabu, and southwards towards Kuh-e-Hoseynabad, and we have inferred that the active faulting extends along these margins (Fig. 13). No scarps are visible in Quaternary alluvium along the margin of either of these two N–S ranges. We note, however, that synclinally folded Neogene basin rocks are present within Kuh-e-Cheng-e-Sabu (Fig. 13; Eftekhar-Nezhad 1977) indicating that uplift and deformation within the range has occurred within the recent geological past. We also note that the local strike of the syncline fold axis, of the topographic expression of Kuh-e-Cheng-e-Sabu, and of the strike of the fault scarp in alluvium, all bend from N–S to NW–SE close

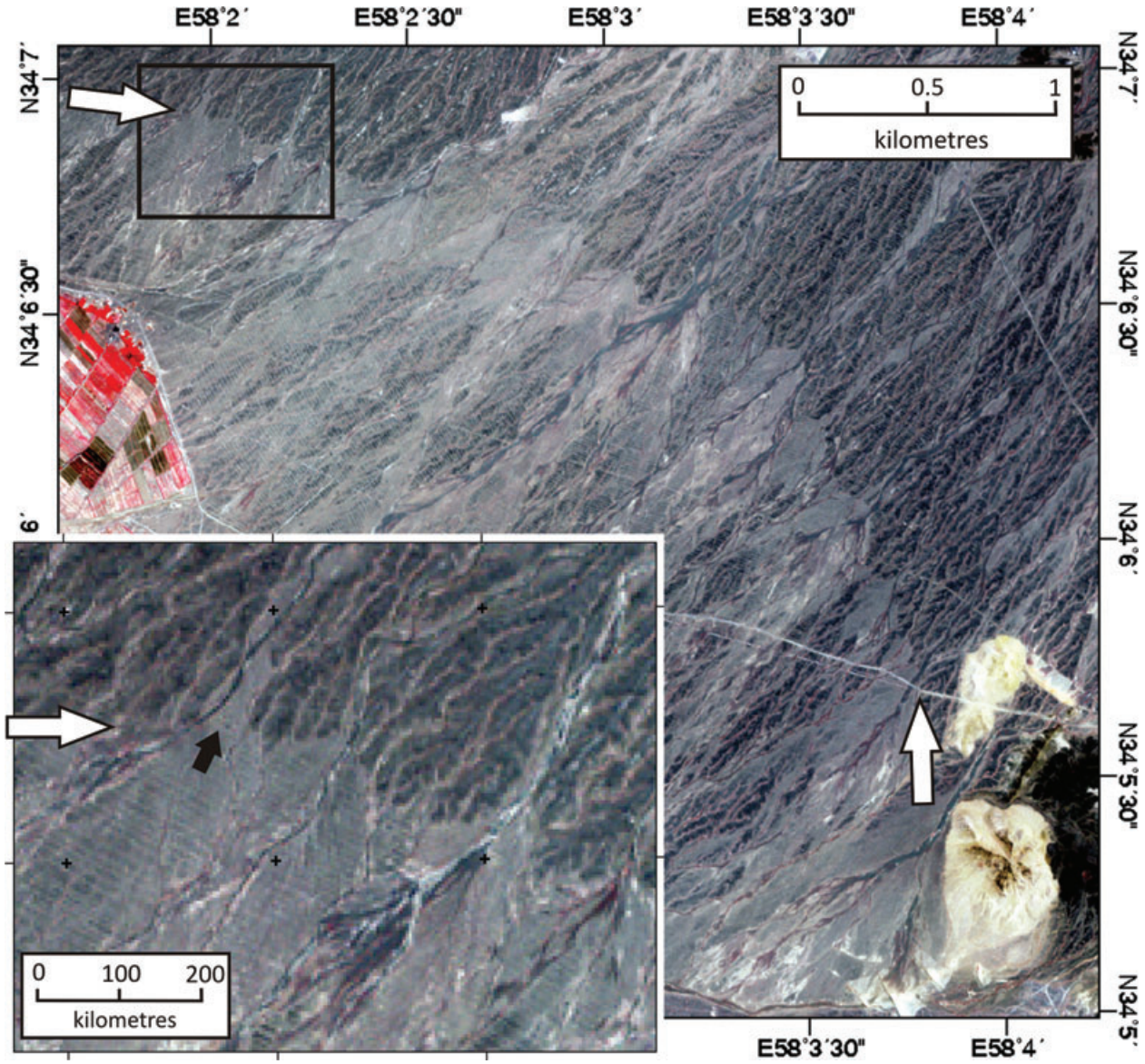

Figure 14. IKONOS satellite image showing a detail of the newly identified scarp (running between the white arrows) in the desert regions west of Ferdows town. Drainage in the regions east and north of the scarp has incised in response to uplift. The inset shows a close-up of the boxed area. No ground deformation is visible where the scarp is crossed by the youngest alluvial fans (at the point highlighted by the black arrow).

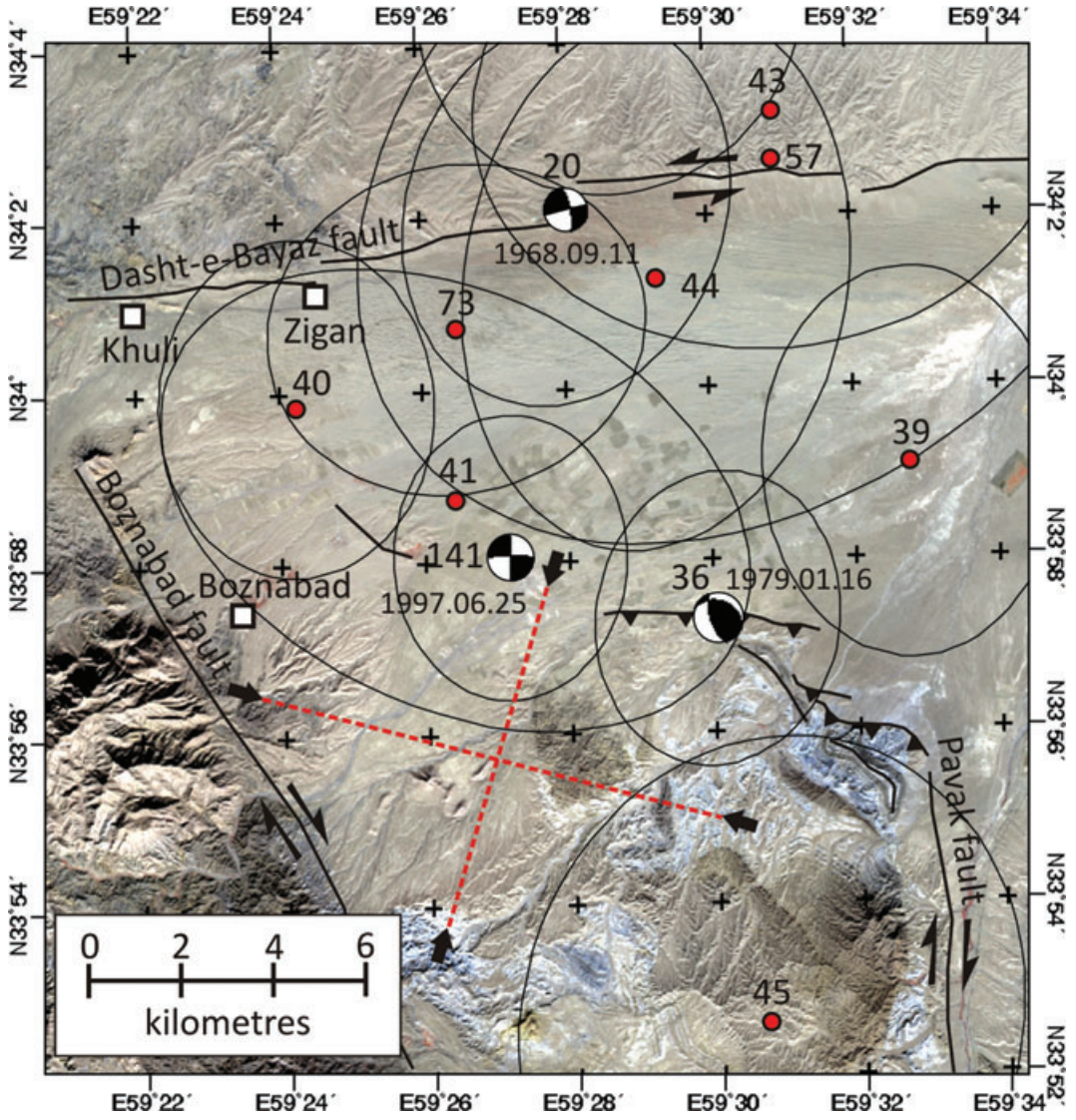

Figure 15. ASTER satellite image of the Boznabad region (see Fig. 1c for location). The E–W left-lateral Dasht-e-Bayaz Fault is visible in the upper part of the image. The 1968 September 11 (#20, M_w 5.6) earthquake is located on the Dasht-e-Bayaz surface trace and it is highly probable that it occurred on this fault. Two roughly N–S right-lateral faults, the Boznabad and Pavak faults, are situated in the lower half. A band of scarps and springs trend E–W across the centre of the image. NW–SE trending folds in bedrock occur in the hangingwall of the E–W scarps. The 1979 January 16 event (#36, M_w 6.5) is sited on the E–W north-facing scarps in a region of NW–SE trending folds in bedrock. Comparison of the fault-plane solution and the exposed faulting and folding indicates that the N–S nodal plane, which dips steeply to the west, is the correct fault plane. The earthquake hence involved oblique reverse and right-lateral faulting. The 1997 June 25 Boznabad earthquake (#141, M_w 5.9) is located in a region of low relief with little in the way of visible active faulting. The pattern of ground deformation imaged by InSAR (Fig. 16) indicates the earthquake occurred on an N–S trending fault. The black arrows and red lines mark the best-fitting fault models for right-lateral and left-lateral slip (Fig. 16). The northern end of the N–S right-lateral model is sited ∼1 km from the epicentre determined from seismology indicating that the earthquake involved slip on an N–S right-lateral fault.

to the location of the 1968 September 1 earthquake, which has NW–SE trending nodal planes (Fig. 13).

5.3 The 1979 and 1997 Boznabad earthquakes

The1979 January 16 event near Boznabad (#36, M_w 6.5) was the first of four destructive earthquakes to occur in that year (Table 1). No surface ruptures were reported following the event, and given the uncertainty in existing single-event epicentral locations (Berberian 1976; Ambraseys 2001), the earthquake has not been tied to any known fault. During the aftershock sequence of the 1997 Zirkuh event, a second destructive earthquake occurred in the Boznabad Plain (1997 June, #141, M_w 5.9). This event destroyed 100 houses, damaged 5000 others and killed some livestock at the villages of Boznabad and Ebrahimabad (Berberian *et al.* 1999; Fig. 15). Berberian *et al.* (1999) suggest, from the distribution of seismic intensities, that faulting in both earthquakes was most likely to have occurred on the N–S trending nodal planes. A series of aftershocks (events #37–46) immediately following the 1979 Boznabad event (Fig. 6b) show a general N–S alignment extending to the north side of the Dasht-e-Bayaz Fault, which might indicate an N–S fault plane, but the pattern is diffuse.

The locations of active faults within the Boznabad plain are marked on Fig. 15. In the south of the image, the faulting is dominated by the N–S right-lateral Boznabad and Pavak faults. Both of these faults show uplift on their western sides that has led to the

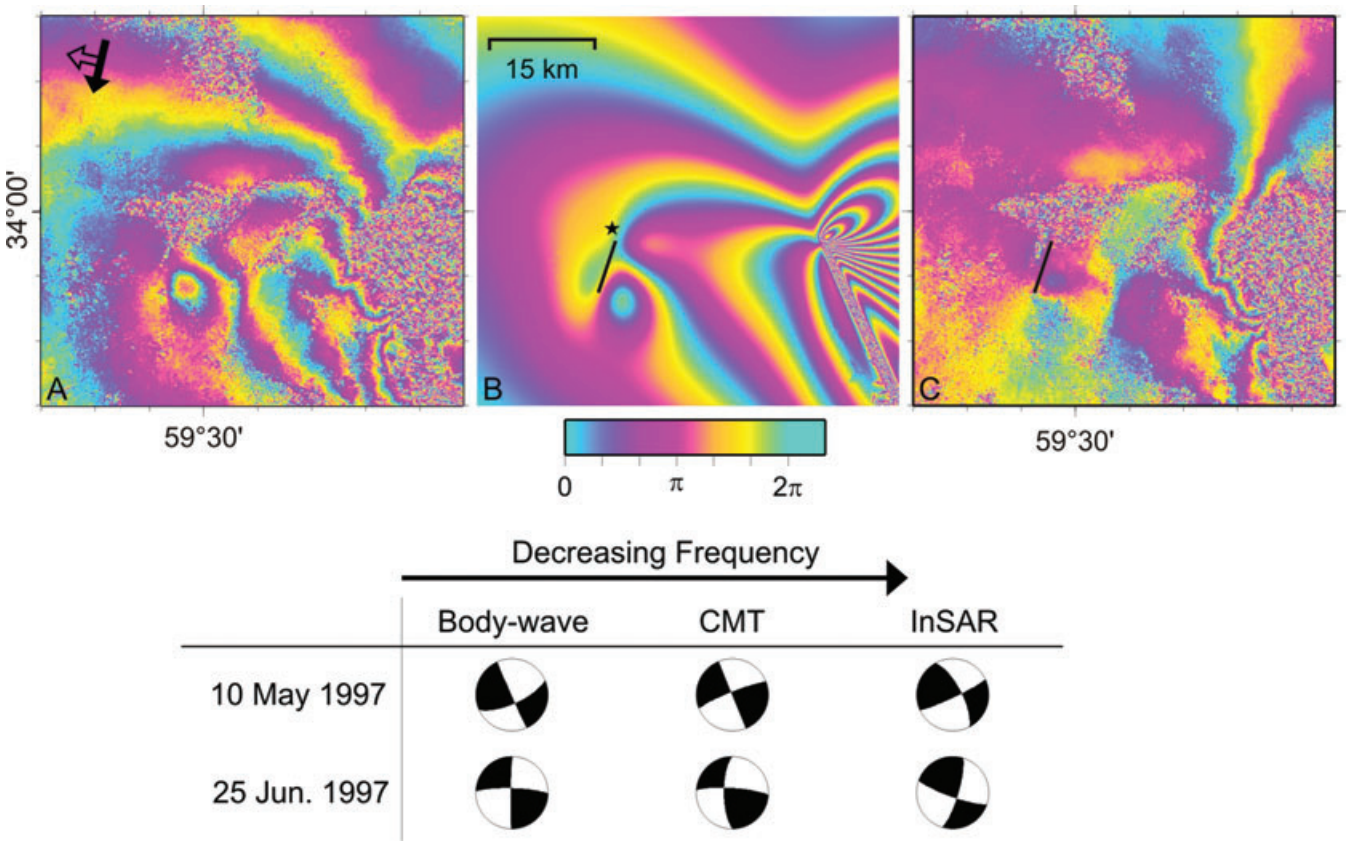

Figure 16. (a) ERS-1 interferogram showing deformation from the M_w 7.2, 1997 May 10 Zirkuh (#92) earthquake plus the 1997 June 25 M_w 5.9 Boznabad earthquake, an aftershock of the 10th May event. Solid arrow indicates the flight direction of the satellite and outlined arrow denotes the look direction of the satellite. (b) Preferred coseismic elastic dislocation model for the 1997 June 25 aftershock with a simplified, single fault approximation for the M_w 7.2 Zirkuh earthquake. The black star indicates the HDC location of the aftershock and the black line denotes the fault identified from inversion of 'a'. (c) Interferogram with coseismic model removed. The black line denotes the fault identified from inversion of 'a'. (d) Graphical comparison of moment tensor solutions from inversion of teleseismic body-wave data (Berberian *et al.* 1999), the Global CMT (Dziewonski *et al.* 1981) and inversion of InSAR data. Each inversion method is sensitive to deformation in different frequency bands. To illustrate this, moment tensors are arranged, from left to right, in order of sensitivity to decreasing frequencies (increasing periods) of radiated energy.

exhumation of bedrock. The Pavak Fault is truncated at its northern end by a series of E–W north-facing scarps. Tightly folded bedrock, with fold axes trending NW–SE, is exposed south of these scarps. Farther to the west, two small oases are aligned along a short E–W south-facing fault scarp. The dominant faulting at the northern edge of Fig. 15 is the E–W left-lateral Dasht-e-Bayaz Fault.

Body-waveform modelling of the 1979 Boznabad event indicates a complicated rupture with two subevents, the first involving NW-striking reverse faulting, and the second showing either N–S right-lateral or E–W left-lateral slip (Baker 1993; Berberian *et al.* 1999). The relocated epicentre of the earthquake is centred on an E–W north-facing scarp. NW–SE trending fold axes exposed in the uplifted southern side of the E–W scarp are compatible with the source parameters of the first subevent of this earthquake. This subevent of the earthquake is hence likely to have involved slip on an SW–dipping reverse fault. Distinguishing between the E–W and N–S nodal planes in the second subevent is more difficult as the epicentre is very close to both the N–S Pavak Fault and the E–W trending structures that truncate the Pavak Fault at its northern end.

The fault-plane solution for the 1997 June 25 Boznabad earthquake indicates either right-lateral slip on an N–S fault or left-lateral slip on an E–W fault. The relocated epicentre of this event is situated within the Boznabad plain. The epicentre is situated only 2 km east of a subtle E–W trending scarp with a series of small springs at its base (Fig. 15). It is also situated a similar distance north of N–S trending structures exposed in bedrock (Fig. 15). The epicentral location and focal mechanism are insufficient on their own to identify the causative fault.

Additional constraint on the source of the 1997 June 25 Boznabad earthquake is provided from a map of the associated ground deformation based on an InSAR analysis (Fig. 16). The interferogram in Fig. 16(a) is constructed from descending-pass ERS-1 scenes from 1992 November 1 and 1998 September 30 with each fringe corresponding to 28 mm of change in range between the satellite and the ground surface. Processing was performed with the JPL/Caltech ROI_pac (Repeat Orbit Interferometry Package) software (Rosen *et al.* 2004) and used the Delft ODR orbits and the SRTM digital topographic data. The long time interval between the ERS-1 scenes covers both the 1997 Boznabad event and the much larger 1997 May 10 Zirkuh main shock that interferes with, and partially obscures, the signal from the smaller event. In our elastic dislocation models, we have approximated the Zirkuh main shock by a single fault-plane trending NNW–SSE and dipping steeply to the east (Fig. 16b; Table 4). The Zirkuh earthquake rupture was complex, involving multiple subevents with differing source parameters (e.g. Berberian *et al.* 1999; Sudhaus & Jónsson 2011) and

Table 4. Source parameters of the 1997 June 25 Boznabad earthquake obtained from elastic dislocation modelling (see Section 5.3).

	Strike	Dip	Rake	Average slip	Length	Top	Base
Dextral	15	60	171	0.25	10.2	3.2	8.2
Sinistral	105	90	7	0.35	10.2	3.2	8.2

our simple fault model leaves a residual signal around the Zirkuh Fault (Fig. 16c). The simple single-fault model for the Zirkuh earthquake is effective, however, in removing distal parts of the pattern of fringes resulting from the Zirkuh main shock. It is these distal fringes that obscure the ground deformation from the Boznabad earthquake and their removal allows us to generate a fault model for the Boznabad earthquake.

Estimation of the fault model from the InSAR data in Fig 16(a) was performed after subsampling of the unwrapped interferogram using a resolution-based methodology (Lohman & Simons 2005b). The best-fitting fault plane was then inverted for using Powell's conjugate gradient descent method with Monte Carlo restarts (Powell 1964; Clarke *et al.* 1997; Funning *et al.* 2007). In testing for the possibility that the earthquake occurred on an E–W oriented sinistral fault, we were required to place tight *a priori* constraints on the strike of the fault. Failure to do so resulted in the solution converging towards the N–S oriented dextral fault solution. The resulting best-fitting sinistral solution showed larger residuals, further suggesting that the rupture had occurred on the N–S trending dextral fault plane. Additionally, the calibrated epicentral location for the Boznabad event is sited at the northern end of the N–S dextral fault model whereas the E–W sinistral fault model is located at least 5 km south of the epicentre (Fig. 15). These two observations, along with the macroseismic data of Berberian *et al.* (1999), suggest that slip in the 1997 Boznabad earthquake probably occurred on an N–S fault plane. The endpoints of the best-fitting fault model are shown in Fig. 15 as black arrows. The epicentral location at the northern end of the modelled rupture is indicative of southward rupture propagation.

5.4 The 1979 Kalat-e-Shur earthquake

The Kalat-e-Shur earthquake (1979 December 7, #68, M_w 5.9) occurred during the aftershock sequence of the Khuli-Buniabad main shock. It is considered separately here because this event has been cited as the cause of rupture observed on the northern Abiz Fault. Roughly 15 km of right-lateral surface rupture on the Abiz Fault, from Kalat-e-Shur northwards to Donakhi (Fig. 9), have been attributed to this earthquake (Berberian & Yeats 1999; Berberian *et al.* 1999). The ruptures were not present following the 1979 November 14 Korizan earthquake (Nowroozi & Mohajer-Ashjai 1980; Mohajer-Ashjai *et al*. 1981). No field investigations were undertaken between November 27 and December 7, the dates of the Khuli-Buniabad main shock and the Kalat-e-Shur event. The ruptures were discovered and mapped by Haghipour & Amidi (1980).

The relocated epicentre of the Kalat-e-Shur event is at the eastern margin of Kuh-e-Kheybar, ∼10 km northeast of Donakhi, and north of the Dasht-e-Bayaz fault trace (Fig. 9). Two aftershocks on the same day (events #69 and #70) are co-located with it. This epicentral area was also active immediately before the Khuli-Buniabad main shock, including just 10 hr before the main shock (1979 November 23, #53, m_b 5.0 and 1979 November 27, #54, m_b 5.1).

There are indications of discontinuous N–S right-lateral faulting in Quaternary alluvium along the eastern margin of Kuh-e-Kheybar (Fig. 17), including the section adjacent to the relocated epicentre of the 1979 December 7 event. From its epicentral location, and from the identification of nearby N–S scarps in Quaternary alluvium, we suggest that the 1979 December 7 earthquake involved rupture on N–S right-lateral faults along the eastern margin of Kuh-e-Kheybar. Given its modest magnitude (M_w 5.9) and the distance from the site of the surface faulting mapped by Haghipour & Amidi (1980), it is unlikely that this event is the cause, and the name 'Kalat-e-Shur' for this event is misleading. We believe that the most likely cause of the ruptures mapped on the Abiz Fault between Kalat-e-Shur and Donakhi (Haghipour & Amidi 1980) is a major subevent during the rupture of the Khuli-Buniabad main shock. Body-waveform modelling of the Khuli-Buniabad main shock indicates the existence of multiple subevents, but the details of each could not be resolved (Walker *et al.* 2004).

6 DISCUSSION

Our combined analysis of earthquake locations and of high-resolution satellite imagery of the epicentral regions has provided a much clearer image of the faulting in this part of Iran, and we have been able to correlate each major event with its probable causative fault.

Of particular note in the late 20th century earthquake sequence is the occurrence of rupture on adjacent conjugate faults. Our calibrated epicentres support a simultaneous rupture of left-lateral and right-lateral faults during the 1979 November 27 Khuli-Buniabad earthquake. Rupture of adjacent left- and right-lateral faults in events separated by several years is observed between the western segment of the left-lateral Dasht-e-Bayaz fault (which ruptured in 1968) and the N–S right-lateral Boznabad and Pavak faults (which failed in 1979 and 1997). Left-lateral slip on the eastern Dasht-e-Bayaz fault during the 1979 Khuli-Buniabad earthquake was followed 18 years later by 125 km of rupture on the right-lateral Abiz Fault in the 1997 Zirkuh earthquake.

Other continental examples where rupture has occurred on adjacent conjugate strike-slip faults include the 1987 Superstition Hills sequence of southern California (Hudnut *et al.* 1989); the 1994 and 2004 Al Hoceima earthquakes in Morocco (Biggs *et al.* 2006) and the sequence of earthquakes on the Bingol and east Anatolian faults of eastern Turkey (Milkereit *et al.* 2004). In each of these sequences, one of the two conjugate fault directions can be picked out as the dominant direction, suggesting that one population of faults has grown at the expense of the other (e.g. Biggs *et al.* 2006). In the sequence of earthquakes on the Dasht-e-Bayaz and Abiz faults, it is rather difficult to say which, if any, of the two fault orientations is dominant. The E–W Dasht-e-Bayaz fault appears to dominate over the adjacent N–S Boznabad, Pavak and Abiz faults (the Abiz Fault, in particular, was separated from right-lateral faults that continue north of it by an uninterrupted left-lateral rupture on the Dasht-e-Bayaz Fault in 1979). The 1997 rupture on the Abiz Fault, however, broke across several E–W left-lateral faults along its length (see Fig. 11). The competition for dominance between E–W left-lateral faults and N–S right-lateral faults in this part of northeast Iran is likely to result from a combination of the active tectonics (involving N–S right-lateral shear), and the inherited geology (which is dominated by structures trending E–W). The competition results in cross-cutting structures that are kinematically unstable and must evolve rapidly.

We have found that many of the events in the 1968–1997 earthquake sequences were caused by slip on faults distributed widely across the region, including several that were not previously known. Although there is an abundant historic record of earthquakes in the

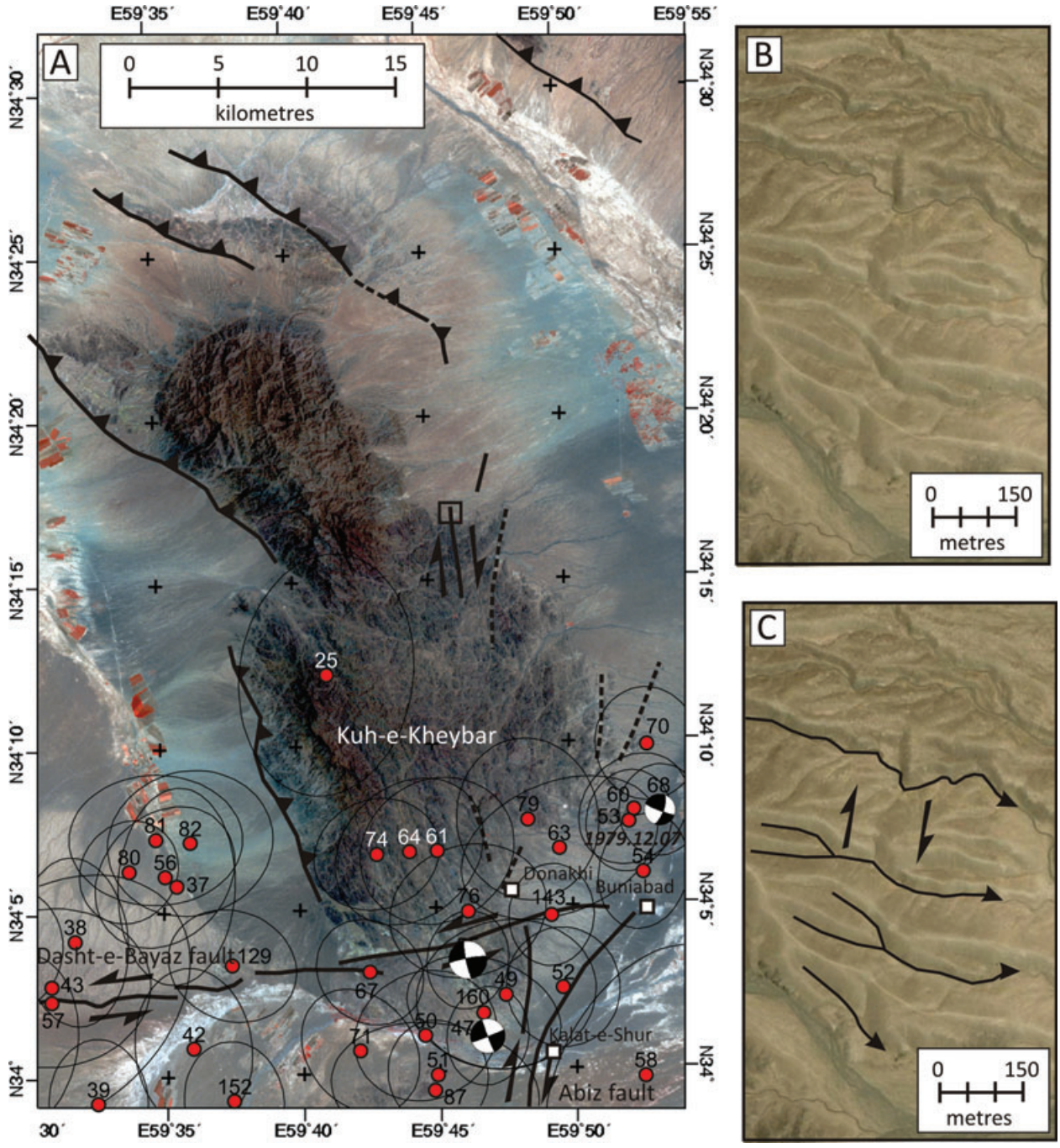

Figure 17. Landsat image of faults around Kuh-e-Kheybar north of the intersection between the Dasht-e-Bayaz and Abiz faults (see Fig. 1c for location). The western margin of Kuh-e-Kheybar is bounded by active thrust faults. Discontinuous faults, with lines of springs supporting small villages, are visible along the eastern margin of the mountain. (b) An enlargement of the boxed region in (a) using SPOT5 imagery from Google Earth. Streams incised into a heavily eroded fan in the southern half of the image show apparent right-lateral deflections of several tens of metres. No deformation is visible in the less dissected fan surface at the north of the image. In (c), the stream channels and the fault location have been annotated for clarity.

area, there is nothing to suggest that any of these historic events represent earlier cycles of rupture on the Dasht-e-Bayaz and Abiz faults. We also note that the geomorphology of the Dasht-e-Bayaz Fault, in particular, is rather subdued and, if it were not for the 1968 and 1979 earthquakes, it would not be picked as a major feature over its neighbours. We therefore postulate that the high concentration of destructive earthquakes in this part of Iran is more to do with the complex faulting in the region, with many short fault segments that interact with one another, rather than rapid slip rates and short recurrence intervals on a few major faults. Interactions within a population of many short fault segments might also help to explain other examples of temporally clustered earthquakes in Iran, such as the sequence of historical and instrumental events east of Kerman city (e.g. Nalbant *et al.* 2006; Walker *et al.* 2010).

The exact nature of the interactions between the faults within our study area is not easy to determine. The transfer of stress is often invoked to explain temporal clustering of earthquakes within a small geographical region (e.g. Stein *et al.* 1995). However, the majority of

the later ruptures in the Dasht-e-Bayaz/Zirkuh earthquake sequence, including that generated by the M_w 7.1 Zirkuh earthquake, appear to have occurred in regions that should have been taken further from failure by the preceding events. Although the improved epicentres that we have presented aid in constraining the sources of each of the destructive earthquakes in the sequence, they constitute only the first step in investigating the cause of this remarkable cluster of earthquake activity, and there is much more to be learnt from further investigation of the origin of the sequence.

7 CONCLUSIONS

The 1968–1997 Dasht-e-Bayaz/Zirkuh sequence of destructive earthquakes in Iran constitutes one of the most outstanding examples of temporally clustered continental seismic activity in the world. Studies of it have, until now, suffered from a lack of constraint on which of the many known faults in the region were active in particular events. Calibrated relocation of epicentres, combined with a regional survey of high-resolution satellite imagery, has helped to remedy this problem and allow the major causative faults to be identified with a reasonably high degree of confidence. The approach that we have used in this investigation is particularly valuable in the study of clustered earthquakes that have occurred prior to the development of InSAR techniques for imaging earthquake ground deformation, and in inaccessible regions where detailed field investigations are difficult. The large amount of seismic activity in this part of Iran results from an inherently unstable arrangement of competing left- and right-lateral faults, which has led to a widespread population of interacting segmented faults, rather than slip being localized onto a small number of structures.

ACKNOWLEDGMENTS

We thank the University of Birjand, the University of Tehran and the Geological Survey of Iran for their support of our work in Iran and for enabling us to visit the Dasht-e-Bayaz region on several occasions. Part of the research described in this paper was performed at the Jet Propulsion Laboratory, California Institute of Technology under contract with the National Aeronautics and Space Administration. IKONOS satellite imagery was provided by the European Space Agency through project allocation No. C1P.6462. We also thank the NERC-funded COMET+ centre in the UK. RTW is supported by a University Research Fellowship from the Royal Society of London.

REFERENCES

Ambraseys, N.N., 2001. Reassessment of earthquakes, 1900–1999, in the Eastern Mediterranean and the Middle East, *Geophys. J. Int.,* **145,** 471–485.

Ambraseys, N.N. & Melville, C.P., 1982. *A History of Persian Earthquakes,* Cambridge University Press, Cambridge.

Ambraseys, N.N. & Tchalenko, J.S., 1969. The Dasht-e-Bayaz (Iran) earthquake of August 31, 1968: a field report, *Bull. seism. Soc. Am.,* **59,** 1751–1792.

Baker, C., 1993. Active seismicity and tectonics of Iran, *PhD thesis*, University of Cambridge, Cambridge.

Berberian, M., 1976. *Contribution to the Seismotectonics of Iran* (Part II), Geological Survey of Iran, Report No. 39.

Berberian, M., 1979. Evaluation of instrumental and relocated epicentres of Iranian earthquakes, *Geophys. J. R. astr. Soc.,* **58,** 625–630.

Berberian, M. & Yeats, R.S., 1999. Patterns of historical earthquake rupture in the Iranian Plateau, *Bull. seism. Soc. Am.,* **89,** 120–139.

Berberian, M. & Yeats, R.S., 2001. Contribution of archaeological data to studies of earthquake history in the Iranian Plateau, *J. Struct. Geol.,* **23,** 563–584.

Berberian, M., Jackson, J.A., Qorashi, M., Khatib, M.M., Priestley, K., Talebian, M. & Ghafuri-Ashtiani, M., 1999. The 1997 May 10 Zirkuh (Qa'enat) earthquake (M_w 7.2): faulting along the Sistan suture zone of eastern Iran. *Geophys. J. Int.,* **136,** 671–694.

Biggs, J., Bergman, E., Emmerson, B., Funning, G.J., Jackson, J., Parsons, B. & Wright, T.J., 2006. Fault identification for buried strike-slip earthquakes using InSAR: the 1994 and 2004 Al Hoceima, Morocco earthquakes, *Geophys. J. Int.,* **166,** 1347–1362.

Bondár, I., Myers, S.C., Engdahl, E.R. & Bergman, E.A., 2004. Epicentre accuracy based on seismic network criteria, *Geophys. J. Int.,* **156,** 1–14.

Bondar, I., Bergman, E., Engdahl, E.R., Kohl, B., Kung, Y-L. & McLaughlin, K., 2008. A hybrid multiple event location technique to obtain ground truth event locations, *Geophys. J. Int.,* **175,** 185–201.

Clarke, P.J., Paradisses, D., England, P.C., Parsons, B., Billiris, G., Veis, G. & Ruegg, J.-C., 1997. Geodetic investigation of the 13 May Kozani—Grevena (Greece) earthquake, *Geophys. Res. Lett.,* **24,** 707–710.

Dziewonski, A.M., Chou, T.-A. & Woodhouse, J.H., 1981. Determination of earthquake fault parameters from waveform data for studies of global and regional seismicity, *J. Geophys. Res.,* **86,** 2825–2852.

Eftekhar-Nezhad, J., 1977. *Geological Quadrangle Map, Ferdows Sheet (No. J6), 1:250,000 scale*, Geological Survey of Iran, Tehran.

Engdahl, E.R., van der Hilst, R. & Buland, R., 1998. Global teleseismic earthquake relocation with improved travel times and procedures for depth determination. *Bull. seism. Soc. Am.,* **88,** 722–743.

Engdahl, E.R., Bergman, E.A. & Myers, S.C., 2008. Seismotectonics of the Iran region, *EOS, Trans. Am. geophys. Un.,* **89**(53), Fall Meet. Suppl., Abstract T23D-06.

Farr, T.G. & Kobrick, M., 2000. Shuttle Radar Topography Mission produces a wealth of data, *EOS, Trans. Am. geophys. Un.,* **81,** 583–585.

Funning, G.J., Parsons, B. & Wright, T.J., 2007. Fault slip in the 1997 Manyi Tibet earthquake from linear elastic modelling of InSAR displacements, *Geophys. J. Int.,* **169,** 988–1008.

Haghipour, A. & Amidi, M., 1980. The November 14 to December 25, 1979 Ghaenat earthquakes of northeast Iran and their tectonic implications, *Bull. seism. Soc. Am.,* **70,** 1751–1757.

Hudnut, K.W., Seeber, L. & Pacheco, J., 1989. Cross-fault triggering in the November 1987 Superstition Hills earthquake sequence, Southern California, *Geophys. Res. Lett.,* **16,** 199–202.

Ikeda, Y., Imaizumi, T., Sato, H., Hessami, Kh. & Khatib, M.M., 1998. Surface faults associated with the Qayen, northeast Iran earthquake of May 10, 1997, *Active Fault Res.,* **18,** 1–13.

Jackson, J., 2001. Living with earthquakes: know your faults, *J. Earthq. Eng.,* **5**(1), 5–123.

Jackson, J.A. & Fitch, T.J., 1979. Seismotectonic implications of relocated aftershock sequences in Iran and Turkey, *Geophys. J. R. astr. Soc.,* **57,** 209–229.

Jackson, J. & McKenzie, D., 1984. Active tectonics of the Alpine-Himalayan belt between Turkey and Pakistan, *Geophys. J. R. astr. Soc.,* **77,** 185–264.

Jordan, T.H. & Sverdrup, K.A., 1981. Teleseismic location techniques and their application to earthquake clusters in the south-central Pacific, *Bull. seism. Soc. Am.,* **71,** 1105–1130.

Lohman, R.B. & Simons, M., 2005a. Locations of selected small earthquakes in the Zagros mountains, *Geochem. Geophys. Geosyst.,* **6,** Q03001, doi:10.1029/2004GC000849.

Lohman, R.B. & Simons, M., 2005b. Some thoughts on the use of InSAR data to constrain models of surface deformation: noise structure and data downsampling, *Geochem. Geophys. Geosyst.,* **6,** doi:10.1029/2004GC000841.

McKenzie, D., 1972. Active tectonics of the Mediterranean region. *Geophys. J. R. astr. Soc.,* **30,** 109–185.

Meyer, B. & Le Dortz, K., 2007. Strike-slip kinematics in Central and Eastern Iran: estimating fault slip-rates averaged over the Holocene, *Tectonics,* **26,** TC5009, doi:10.1029/2006TC002073.

Milkereit, C., Grosser, H., Wang, R., Wetzel, H-U., Woith, H., Karakisa, S., Zunbul, S. & Zscau, J., 2004. Implications of the 2003 Bingoel Earthquake for the interaction between the North and East Anatolian faults, *Bull. seism. Soc. Am.,* **94,** 2400–2406.

Mohajer-Ashjai, A., Nowroozi, A.A., Taghi-Zadeh, Gh. & Zohurian,-Izadpanah, A.A., 1981. *A Report on the Twin Earthquakes in Qayenat*, Atomic Energy Organisation of Iran, Report no. 122 (in Persian).

Nalbant, S.S., Steacy, S. & McCloskey, J., 2006. Stress transfer relations among the earthquakes that occurred in Kerman province, southern Iran since 1981. *Geophys. J. Int.,* **167,** 309–318.

Nissen, E., YaminiFard, F., Tatar, M., Gholamzadeh, A., Bergman, E., Elliott, J., Jackson, J. & Parsons, B., 2010. The vertical separation of mainshock rupture and microseismicity at Qeshm island in the Zagros Simply Folded Belt, Iran, *Earth. planet. Sci. Lett.,* **296,** 181–194.

Nowroozi, A.A. & Mohajer-Ashjai, A., 1980. Faulting of Kurizan and Koli (Qaenat Iran) earthquakes of November 1979: a field report, *Iran. Pet. Inst. Bull.,* **78,** 8–20.

Parsons, B. *et al*., 2006. The 1994 Sefidabeh (eastern Iran) earthquakes revisited: new evidence from satellite radar interferometry and carbonate dating about the growth of an active fold above a blind thrust fault, *Geophys. J. Int.,* **164,** 202–217.

Powell, M.J.D., 1964. An efficient method for finding the minimum of a function of several variables without calculating derivatives, *Comput. J.,* **7,** 152–162.

Ritzwoller, M.H., Shapiro, N.M., Levshin, A.L., Bergman, E.A. & Engdahl, E.R., 2003. Ability of a global three-dimentional model to locate regional events, *J. geophys. Res.,* **108,** 2353, doi:10.1029/2002JB002167.

Rosen, P.A., Hensley, S., Peltzer, G. & Simons, M., Updated Repeat Orbit Interferometry Package released, *EOS, Trans. Am. geophys. Un.,* **85,** 47, doi:10.1029/2004EO050004.

Stein, R.S., King, G.C.P. & Lin, J., 1995. Stress triggering of earthquakes: evidence for the 1994 M = 6.7 Northridge, California, shock, *Ann. Geofis.,* **37,** 1799–1805.

Sudhaus, H. & Jónsson, S., 2011. Source model for the 1997 Zirkuh earthquake (M_w = 7.2) in Iran derived from JERS and ERS InSAR observations, *Geophys. J. Int.,* **185,** 676–692, doi:10.1111/j.1365-246X.2011.04973.x.

Tatar, M., Jackson, J., Hatzfeld, D. & Bergman, E., 2007. The 2004 May 28 Baladeh earthquake (M_w 6.2) in the Alborz, Iran: overthrusting the South Caspian Basin margin, partitioning of oblique convergence and the seismic hazard of Tehran, *Geophys. J. Int.,* **170,** 249–261.

Tchalenko, J.S. & Ambraseys, N.N., 1970. Structural analysis of the Dasht-e-Bayaz (Iran) earthquake fractures, *Bull. geol. Soc. Am.,* **81,** 41–60.

Tchalenko, J.S. & Berberian, M., 1975. Dasht-e-Bayaz fault, Iran: earthquake and earlier related structures in bed-rock, *Bull. geol. Soc. Am.,* **86,** 703–709.

Vernant, P. *et al*., 2004. Present-day crustal deformation and plate kinematics in the Middle East constrained by GPS measurements in Iran and northern Oman, *Geophys. J. Int.,* **157,** 381–398.

Walker, R. & Jackson, J., 2004. Active tectonics and late Cenozoic strain distribution in central and eastern Iran, *Tectonics,* **23,** TC5010, doi:10.1029/2003TC001529.

Walker, R.T. & Khatib, M.M., 2006. Active faulting in the Birjand region of NE Iran, *Tectonics,* **25,** TC4016, doi:10.1029/2005TC001871.

Walker, R., Jackson, J. & Baker, C., 2003. Thrust faulting in eastern Iran: source parameters and surface deformation of the 1978 Tabas and 1968 Ferdows earthquake sequences, *Geophys. J. Int.,* **152,** 749–765.

Walker, R., Jackson J. & Baker, C., 2004. Active faulting and seismicity of the Dasht-e-Bayaz region, eastern Iran. *Geophys. J. Int.,* **157,** 265–282.

Walker, R.T., Bergman, E., Jackson, J., Ghorashi, M. & Talebian, M., 2005. The 2002 June 22 Changureh (Avaj) earthquake in Qazvin province, northwest Iran: epicentral relocation, source parameters, surface deformation and geomorphology, *Geophys. J. Int.,* **160,** 707–720.

Walker, R.T., Talebian, M., Saiffori, S., Sloan, R.A., Rasheedi, A., MacBean, N. & Ghassemi, A., 2010. Active faulting, earthquakes, and restraining bend development near Kerman city in southeastern Iran, *J. Struct. Geol.,* **32,** 1046–1060.